Analyzing failure behavior and prediction models for LH2 fuel tank

Auteur : Sanchez Mogrovejo, Esteban Alexander
Promoteur(s) : Rigo, Philippe
Faculté : Faculté des Sciences appliquées
Diplôme : Master : ingénieur civil mécanicien, à finalité spécialisée en "Advanced Ship Design"
Année académique : 2023-2024
URI/URL : http://hdl.handle.net/2268.2/22261

Analyzing Failure Behavior and Prediction Models for LH2 Fuel Tank

submitted on 03 August, 2024

by

SANCHEZ MOGROVEJO Esteban Alexander

Hammer Straße 10

22041 Hamburg

esteban.mogrovejo@uni-rostock.de

Student ID No.: 223 202 145

First Reviewer:

Prof. Dr. Eng./ Hiroshima Univ. Patrick Kaeding

University of Rostock

Chair of Ship Structures

Albert-Einstein-Str. 2

18059 Rostock

Germany

Second Reviewer:

MSc Tanvir Muhammedul

Researcher Scientist

Düneberger Straße 108

21502 Geesthacht

Germany

EMship+
Advanced Design

Master Thesis

TABLE OF CONTENTS

DECLARATION OF AUTHORSHIP

I, SANCHEZ MOGROVEJO Esteban Alexander declare that this thesis and the work presented in it are my own and have been generated by me as the result of my own original research.

Where I have consulted the published work of others, this is always clearly attributed.

Where I have quoted from the work of others, the source is always given. With the exception of such quotations, this thesis is entirely my own work.

I have acknowledged all main sources of help.

Where the thesis is based on work done by myself jointly with others, I have made clear exactly what was done by others and what I have contributed myself.

This thesis contains no material that has been submitted previously, in whole or in part, for the award of any other academic degree or diploma.

I cede copyright of the thesis in favour of the University of Rostock

Date: 03.08.2024   Signature: *Esteban Sanchez*

I

LIST OF ABBREVIATIONS

Abbreviation	Meaning
CAD	Computer-Aided Design
DNV	Det Norske Veritas
FEA	Finite Element Analysis
IGC	International Gas Carrier (often referring to the International Code for the Construction and Equipment of Ships Carrying Liquefied Gases in Bulk)
IMO	International Maritime Organization
LH2	Liquid Hydrogen
LNG	Liquified Natural Gas
SS316L	Stainless Steel 316, Low-carbon variant

LIST OF FIGURES

LIST OF TABLES

ABSTRACT

Great efforts have been made in the maritime industry to reduce its CO2 footprint by transitioning from fossil fuels to alternative fuels. Liquid hydrogen (LH2) has been identified as a promising alternative because of its high energy density, as well as zero emissions. Challenges in infrastructure and storage systems have been identified for this potential fuel. Currently, C-type tank designs are under research to store and ship this fluid. These storage units consist of a set of inner and outer tanks connected by structures such as I-beams or Bakelite supports. While these solutions are suitable for LNG storage, limitations in handling thermal and mechanical stresses emerge when this technology is adopted for LH2.

This study aims to address the research gaps in this matter by proposing a spring arrangement connection between the tanks as one of the potentially feasible solutions. This novel supporting structure is designed to reduce the contact area with the inner tank, thereby decreasing the conduction heat transfer.

Within this study, the vapor pressure and thermal stresses induced by the LH2 cryogenic temperature are considered. The evaluation of the connection systems consists of addressing the fatigue life of the storage tank by employing the stress-life method and the Finite Element Analysis (FEA) for structural stress determination. The methodology involves the evaluation of stress values generated by two loading scenarios, the bunkering process, and the ship's movement. These stress values are then used to determine the fatigue life of the storage unit. Compliance of the results with the IGC code and DNV rules for strength and fatigue resistance is also presented.

The research showed that the spring connection reduced the heat transfer from the outside to the inner tank which reduced thermal stresses induced by the temperature gradient. Moreover, stress limits and fatigue damage experienced by the inner and outer tanks complied with international regulations indicating the spring connection as a favorable alternative.

1. INTRODUCTION

1.1. Literature Review

The adoption of alternative fuels in strategic sectors such as transportation, energy generation, and manufacturing has become crucial for the achievement of the Sustainable Development Goals (SDGs) proposed by the United Nations, being specifically related to the 7th, 9th, and 13th goals. Within transportation sector, maritime segment is one of the most important industries due to its enormous influence on product shipping with a market portion of 80% in volume (Foretich et al. 2021; Cotorcea und Ozkaynak 2014), as well as greenhouse gas emissions of the environment related to fossil fuels with an estimated 3% of the pollution generated by human activity (Wang und Wright 2021; UNCTAD 2018). Significant efforts have been made to palliate the carbon footprint of maritime transportation targeting alternative fuels and operation efficiency. Some of these alternative power sources are LNG, biofuels, electric batteries, solar and wind power, and liquid hydrogen (LH2), among others. Nonetheless, further investigation needs to be done to achieve a feasible transition.

Transition to sustainable and efficient fuels for the maritime industry faces important barriers to overcome. One of the remarkable challenges is the correct implementation of the various alternatives to fossil fuels available nowadays, with each fuel presenting its own set of difficulties. Discussions about the viability of battery electric propulsion have been focused on the energy production supply chain, as well as the challenges of low volumetric and energy density. LNG and biofuels are proposed as suitable alternatives for medium-term transition to a zero-emission fuel. Additionally, biofuels introduce the discussion of affecting food production by competing for lands in its production (Wang und Wright 2021). The problem with solar and wind power relies on the space on board required to install their equipment and the weather conditions to provide energy (Cotorcea und Ozkaynak 2014; Aijjou 2019).

LH2, due to its abundant availability, high energy density, and zero carbon emissions, is presented in this study as a suitable solution. Despite these great characteristics, LH2 comes with problems related to the required bunkering infrastructure and its storage. This difficulty can be mitigated by adapting the LNG facilities, considering the similarities they have in terms of handling requirements. Regarding the storage units, there are regulations presented by

classification societies or the International Maritime Organization (IMO) that classify different types of tanks. According to the IMO classification, there are independent tanks, membrane tanks, integral tanks, and semi-membrane tanks (IGC Code). From this classification, independent tanks are preferred to store LNG and similar liquefied gases because of safety reasons as they are robust and present a self-supporting structure. A further classification in types A, B, and C is defined within the independent tanks. Being the C-type tanks preferred for their simplicity and capacity to handle high pressure (Kim und Chun 2023). A scheme with the basic components of a type C tank is displayed in Figure 1.
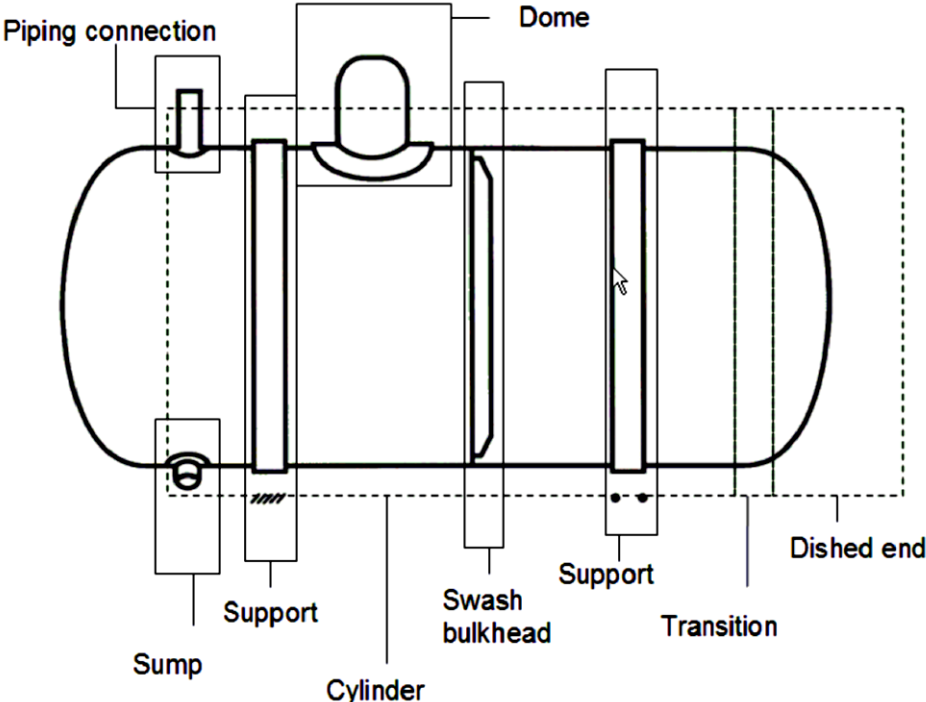
Figure 1. Type C tank components (DNV-CG-0135)

These tank models, borrowed from the LNG industry, are adequate to be adapted for LH2 considering the differences in operational conditions. However, the adaptation process requires more investigation and testing to be fully implemented (Wang und Wright 2021). One aspect that differentiates LNG and LH2 is the capacity of the latter to interact with metals and modify their properties. Considering the conditions of cryogenic temperature and low pressure, in addition to the cycling loads they may experience in their lifespan, problems such as the generation and growth of cracks ending in leaks are matters of concern for metallic vessels regarding safety reasons (Ratnakar et al. 2021). The mechanical properties reduction of metallic materials due to embrittlement effects of hydrogen diffusion in maritime cargo systems has been extensively documented (Kim und Chun 2023; Park et al. 2023). Therefore, it is of great

importance to systematically study the strength and fatigue life of the storage units dedicated to LH2.

The correct analysis of the tank's strength requires two important steps. The first one is the correct selection of the material of each component. For this, specific characteristics need to be set as selection criteria. In the application of LH2, parameters such as suitability to operate at cryogenic temperatures, the effect of hydrogen embrittlement, and high fatigue limit as well as yield and ultimate strength can be selected as deciding factors (Kim und Chun 2023). This group of characteristics narrows down the materials pool of candidates to nickel steel alloys, 300 austenitic stainless-steel series, aluminum alloys from series 5, and high manganese steels according to the ICG and IGF codes. Some additional candidates for hydrogen storage in gas or liquid form that are not listed in the before-mentioned codes are titanium alloys and composite materials such as CFRP (Tomioka et al. 2012; Senthil Kumar et al. 2020). After selecting the material, the second step is comparing the mechanical strength of the material with the resulting stresses produced by the operation conditions. Therefore, analyzing the stress is the next step to address the strength of the tank.

The evaluation of the mechanical characteristics of an LH2 tank requires determination of stresses generated by the internal pressure and temperature, which has been demonstrated to influence the fatigue life of storage vessels (Tomioka et al. 2012). Special care must be taken to identify the resultant maximum stress the tank will bear. This stress could be induced by the combination of the ship's movement loading scenario and the filling process. On top of that, residual stresses from the manufacturing process and material imperfections should also be taken into account (Fricke 2017; Weicheng 2002). In order to consider all the relevant stresses in the strength evaluation, various methodologies could be applied. Analytical methods are the simplest ones, still widely used by virtue of their accuracy and ease of application. Among the theories implemented for fatigue life determination, well-known methods are the Cumulative Fatigue Damage and Fracture Mechanics theories (Weicheng 2002). The latter one has been implemented in the fatigue life evaluation of storage vessels for gaseous hydrogen (Zhou et al. 2016). In the study done by (Zhou et al. 2016), the relation between wall thickness established from different regulations and fatigue life was applied and discussed for low alloy steels, austenitic stainless steels, and iron-based superalloys.

For the Cumulative Fatigue Damage theory, further categorization is needed since it presents different criteria for the evaluation of fatigue life, varying from strain, energy, and stress-based

approaches (Weicheng 2002). The last one is also known as the stress-life method. This strategy uses curves of the number of cycles and the stress range applied to the specimen to predict fatigue life. It considers the particularities of the structural configuration by employing techniques to deal with stress concentrators (Besten 2018). Within the stress-based methodology, the characterization of the stress can be interpreted as a hot spot in geometric zones where there are expected to be increments in the stress value. This approach is one of the most applied in ship structural design and is widely accepted by maritime regulatory entities (Fricke 2017). This technique uses either linear interpolation through-thickness or points located at a specific distance of the study point near the stress concentration zones to compute the stress. The stress value obtained from this process is then introduced in the S-N curves to obtain the fatigue life of the component (Niemi et al. 2018). This method requires the determination of stress values of different points along the surface or thickness. The determination of the stress values of different points along the surface or thickness can be problematic if stress measurement processes are not feasible. Then, tools such as Finite Element Analysis (FEA) show up as an alternative.

Nowadays, the implementation of FEA is an established technique when addressing structural problems steered by the complexity of the analyzed systems and the result concordance with experimental tests (Du-Yong Lee et al. 2023). In fatigue life determination, FEA is usually supported by different analytical methods discussed before (Marzbanrad et al. 2012). Investigation for selecting the design of storage tanks for hydrogen in both liquid and gas states has been carried out using Finite Element Analysis (FEA) (Park et al. 2021). Especial effort has been put into the material selection stage of the tank design by comparing distinct material options such as titanium, steel, aluminum alloys, and composite materials under different pressure conditions to evaluate the structural strength of the tanks (Senthil Kumar et al. 2020; Abinay et al. 2022; Marzbanrad et al. 2012; Du-Yong Lee et al. 2023; Park et al. 2021). These research works display, on the one hand, the viability of the combination of theoretical strategies with the application of FEA for mechanical properties determination. On the other hand, the easiness that computational simulation of LH2 storage tanks presents in determining the feasibility of design modifications considering changes in geometry and materials in comparison to experimental procedures.

Experimental techniques are also used for the purpose of fatigue life estimation. The hydraulic-pressure-cycle test (HPCT) and the hydrogen-gas-cycle test (HGCT) are commonly used for fatigue life assessment for gaseous hydrogen state storage systems. These tests could take from

days for the HPCT to months for the HGCT to be applied and show the influence in fatigue life and stress of hydrogen storage either in tanks made of metals or composite materials (Tomioka et al. 2012; San Marchi et al.). For LH2, additional considerations for testing should be taken, for instance, the extremely low temperature must be added to the hydrogen atmosphere conditions. Equipment that can replicate these conditions is difficult to fabricate, making the investigation in this field complex to achieve (Park et al. 2023). The research in LNG has been prioritized over the past years, contributing to the lack of investigation into hydrogen systems. Additionally, few research studies have focused on its gaseous form to detriment of the LH2. This lack of information, plus few capable facilities represents a barrier to innovation to the increasing demand for this alternative fuel (Park et al. 2023). Extensive efforts need to be performed in the development and optimization of storage units for LH2 in terms of structural, as well as functional aspects.

In this research, the feasibility of a noble supporting structure between the inner and outer tanks is presented aiming to enhance the performance of the storage system. A spring arrangement system will be tested instead of traditional solutions such as I-beam profiles or Bakelite supports. I-beams, commonly used for connecting these components (Bo Wang 2015), displays a large contact area easing the heat transfer from the environment to the inner tank. Supports made of Bakelite, used in type C tanks (Park et al. 2021), have a good performance as insulation material; however, due to its brittle behavior, Bakelite is not suitable for carrying high loads at cryogenic temperatures. The objective of this variation is to reduce thermal conductivity between the tank structures by minimizing the contact area, thereby decreasing heat transfer to the environment. By reducing the heat transfer between the external environment and the internal tank, thermal stresses are expected to decrease. Additionally, this proposed variation reduces the impact of accelerations generated by sea state and ship's operation during transportation. Considering the stress reduction due to thermal variations and accelerations, the fatigue endurance of the tank is expected to improve. Finally, the operational cost of the temperature control system is assumed to decrease thanks to thermal conductivity reduction.

In summary, this study presents the implementation of the structural stress theory aided with FEA to compute stress values in critical points to assess the fatigue life of an LH2 type C storage tank with spring connections between inner and outer tanks. Enclosed by this task, the performance of the spring connection is evaluated as an alternative to the common support structures adopted by LNG storage systems. This investigation intends to contribute to reducing the gaps in available data regarding LH2 storage systems.

1.2. Problem Statement

The adoption of technology from LNG to LH2 has presented several issues due to the difference in storage conditions. Moreover, storage tanks in the maritime industry experience multiple cyclic loads during their lifespan caused by the bunkering process and varying ship's operational conditions. In addition, the harsh environment and operational conditions can significantly reduce the fatigue damage strength of the material, potentially leading to partial or complete failure of the tank's components. Therefore, exploring alternative designs and evaluating the fatigue strength of such critical equipment results in a matter of interest addressed by this research.

1.3. Objectives

This work aims to investigate the fatigue life of an LH2 storing type C tank with spring connections between tanks by using static structural computational simulation to ensure compliance with the IGC code. Followings are carried out to fulfill the purpose of this study:

- Analyzing the performance of the spring connections effect under the applied loading conditions.
- Evaluating the structural and thermal stresses generated due to the cryogenic temperature and vapor pressure resulting from storing LH2 using FEA.
- Evaluating the structural stresses generated due to the ship's movement design loads using FEA.
- Comparing and validating the results with the corresponding international regulations.

1.4. Scope and Limitations

This research targets the implementation of a spring arrangement connection and its fatigue life evaluation centered on the Cumulative Fatigue Damage Theory, specifically in the structural stress-based approach with the FEA as a complement to analyze and retrieve the stress values at high-stress concentration points.

For the loading conditions, vapor pressure acting inside the tank is referenced to previously established literature (Liu et al. 2023). Additionally, the internal temperature of the tank is assumed to be constant at -255°C, corresponding to the temperature of LH2. The accurate pressure value and actual temperature distribution inside the tank require either carrying out a Computational Fluid Dynamics analysis or conducting laboratory experiments. The evaluation of the Boil-off model and the thermal gradient of the inner tank by both methodologies are out of the scope of this research.

Besides the assumptions explained, some challenges were faced during the evaluation process. First, the shortage of investigation regarding LH2 storage tanks represented a considerable limitation during this study. Specifically, studies including the inlet and outlet holes and their effect on the stress distribution of the tank and fatigue life assessment, as well as the implementation of spring connections between inner and outer tanks applied to maritime transportation of LH2. Moreover, high computational power required to perform FEA in such complex models represents barriers to consider for this type of research.

Finally, the resulting conclusions are limited to the geometry, design, and dimensions of the type C tank used in the study, and it is not recommended to be used in a different model. This is because of the dependence on geometric parameters, the boil-off effect, loading and boundary conditions of the tank.

1.5. Thesis Outline

This study is divided into five chapters going through different stages performed to accomplish the proposed objectives. In the first chapter, a brief introduction covering the problem statement is presented. Then, a detailed literature review addressing the efforts that have been put into sustainable fuel adoption and the importance of its application in the maritime industry, highlighting the advantages and challenges of LH2 is presented. This section was intended to contribute to the understanding of the state of the art of LH2 storage tank units. Furthermore, the intentions of the research and the sub-task performed to fulfill them with the limitations encountered during the process are presented.

In chapter two, the methodology employed in this research is explained. The model of the tank with its components is presented. Subsequently, the regulations recommended by the IMO considered in this study for design, strength, and fatigue assessments are introduced.

Chapter three presents the numerical simulations carried out to determine the stress distribution along the LH2 storage tank under different loading cases. Aspects related to the tuning up process of the numerical simulations are explained in this chapter. Moreover, the results of thermal and structural simulations are discussed. This chapter finishes with the compliance analysis of the tank with international standards related to stress limits and fatigue damage.

Following the results and fatigue study, chapter four is dedicated to the discussion and conclusions resulting from the findings and processes performed. Finally, chapter five presents the recommendations and future work motivated by this research.

2. METHODOLOGY

This chapter presents an overview of the processes done in this study which can be summarized in a flowchart displayed in Figure 2. The literature review, presented in the previous chapter, is showcased as the first step and serves to understand the state of the art of LH2 storage technology. Within this investigation phase, relevant data was collected to shape the incoming stages. Materials used in the industry for LNG and LH2 applications, geometry and design of tanks regulated by international standards in the maritime sector, and boundary conditions for the numerical analysis were determined using the information collected through previous research and literatures.

Following the literature review, the design stage is presented. In this section, the SOLIDWORKS 2022 computational package was employed to develop the components and assemble the storage unit. The material selection process is presented as the next step where two variations of the same stainless steel commonly used in LH2 and LNG storage applications were selected. Their relevant properties for stress and fatigue life evaluation are detailed. Both the design process and material selection were conducted in close collaboration with the guidelines specified by the corresponding international regulation. The International Maritime Organization (IMO) developed the International Code for the Construction and Equipment of Ships Carrying Liquefied Gases in Bulk (IGC code). This regulation code set delimitations for the design, construction, operation, and handling of equipment to transport liquefied gases in bulk. In addition, the DNV rules were implemented as the IGC recommends its use in combination with the classification society employed in the vessel. The scantling process, material recommendations, allowable stress limits, and expected fatigue life are specified within the regulation. The significant specifications from the rules are presented in the section following the material selection process.
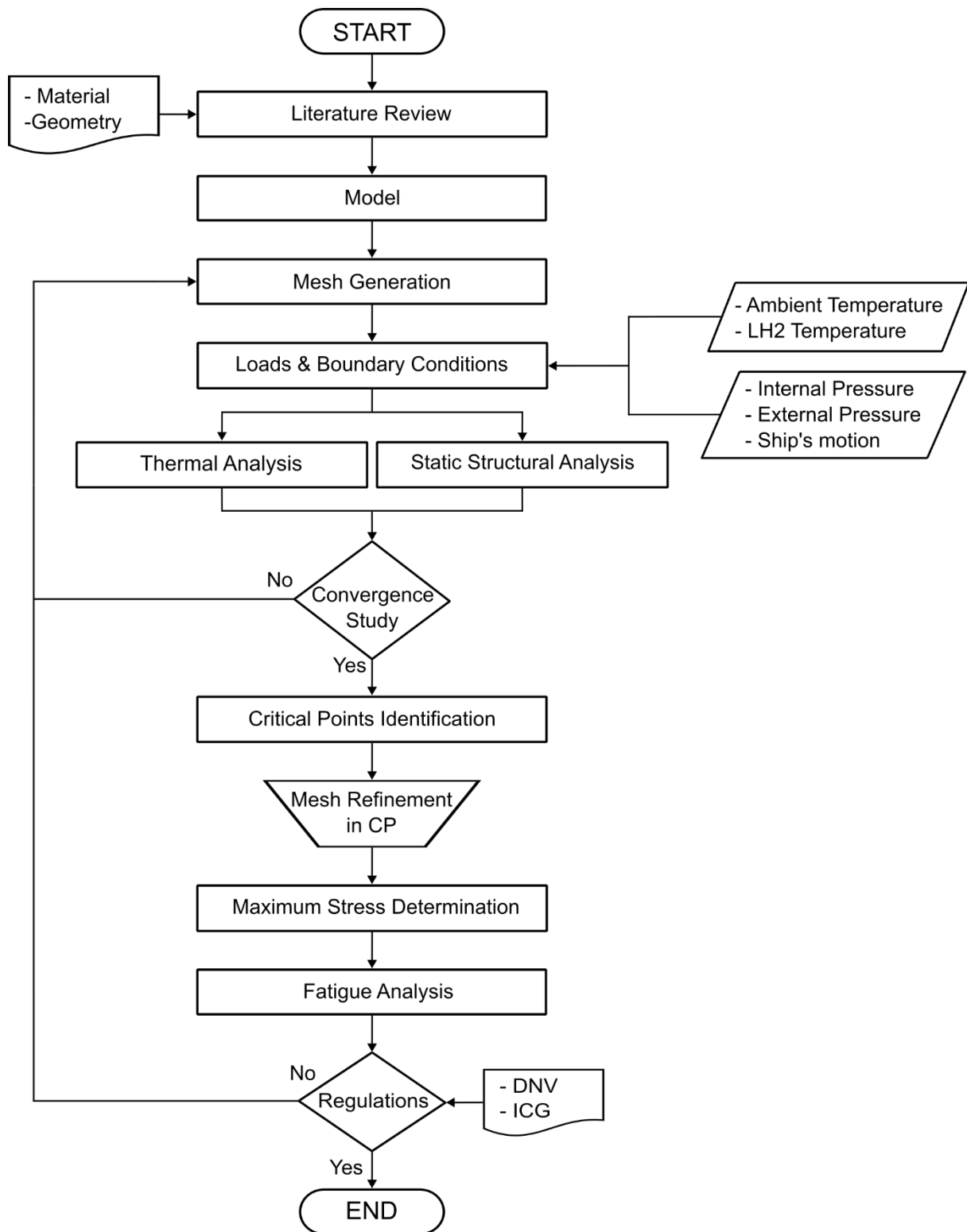
Figure 2. Workflow of the research study

2.1. Tank Model

The selected model is a type C tank compliant with the ICG code part E, section 4.22.7 (IGC Code) and DNV rule part 4, chapter 7 (DNV-RU-SHIP). The 3D model was done in the SolidWorks computational package. The storage unit is made up of two tanks, with both tanks having a cylindrical body and are differentiated by their caps (see Figure 3). The design parameters respond to the operational conditions of each tank. While the inner tank has hemispherical ends to support the pressure generated by the evaporation of the hydrogen, the outer tank was designed with torispherical heads as it will not bear internal pressure. This double barrier configuration is necessary for cryogenic applications to reduce heat transfer with the environment, and it acts as a security barrier in leak scenarios.

For the connection between the tanks, sixteen springs are employed which are aligned in four different orientations. Eight springs are vertically aligned, four at the bottom and four at the top of the inner tank. The other eight springs are divided into two groups aligned at 60° from the vertical at each side of the top of the inner tank. The tank connection is a design proposition and is intended to reduce the heat transfer from the outer to the inner tank. High stress values are expected in the springs because of the applied loads to the system and the thermal gradient produced on them.
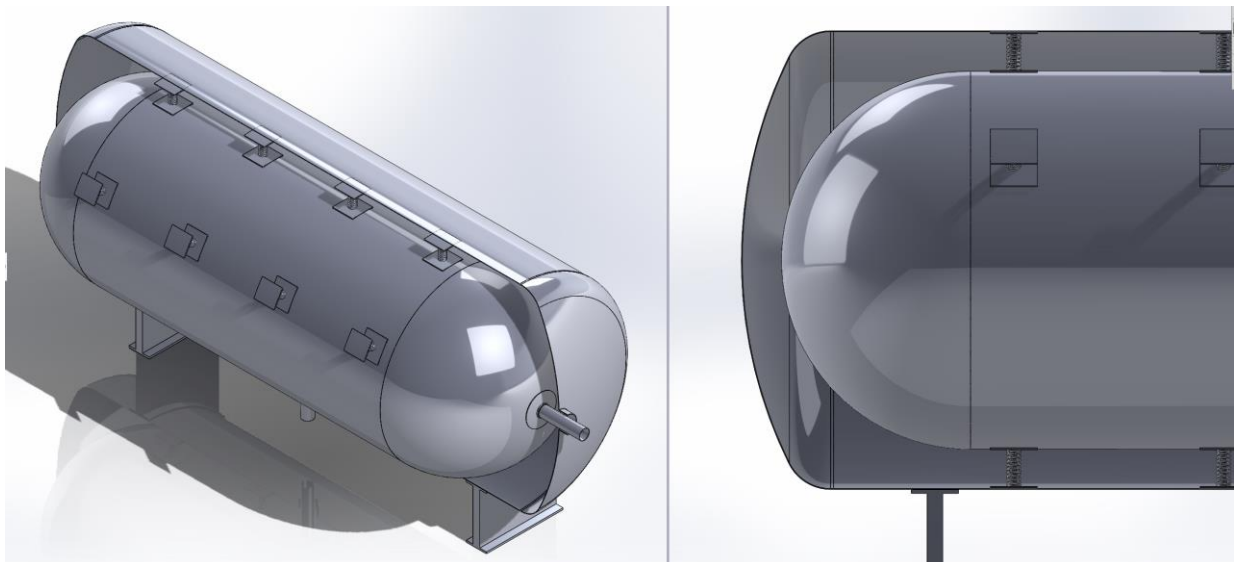
Figure 3. Tank model

Additional elements present in the design are two legs and two connecting plates for each spring, as well as the inlet and outlet pipes and their corresponding reinforcement. Two holes which are located in the hemispherical cap and at the bottom of the inner tank are dedicated to inlet, outlet, or purge line as shown in Figure 4. The locations of these two openings are selected according to the common designs for piping configuration of this type of tank (DNV-CG-0135). According to the safety regulations for pressure tanks (DNV-RU-SHIP), any opening or connection in the element must be reinforced. The reinforcement was made in compliance with the DNV-RU-SHIP Pt.4 Ch.7 rule.
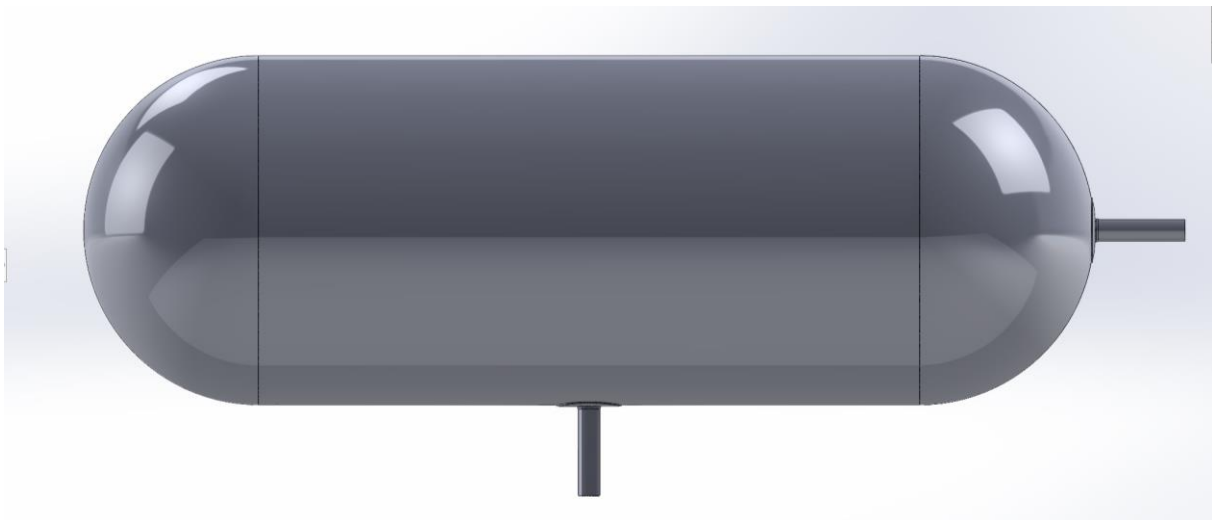
Figure 4. Inner tank piping configuration

It is important to note that the initial design of the tank was developed as part of the research work of the SImTAnk 2 project of the Ship Reliability department of the DLR Institute of Maritime Energy Systems. The author of this study received the tank design and performed modifications to it.

2.2. Material Selection

The window of available materials that can be used for storing LH2 is completely limited to those that can work at cryogenic temperatures, precisely -255° C. Several metallic candidates can be highlighted from the literature review, including austenitic stainless steel, aluminum, and titanium alloys. Among the stainless-steel alloys, austenitic steels such as 304, 316, and 321 are commonly implemented for LH2 applications (Park et al. 2023). For harsh environments prone to produce corrosion, like in maritime applications, low carbon content

variations such as 304L and 316L are preferred. Due to the extensive available data, the SS316L was selected for all the components excluding the springs. This material exhibits relatively low yield and ultimate strength values. Depending on the chemical composition the range for the yield strength goes from 150 to 300 MPa and the ultimate strength ranges from 450 to 620 MPa.

For the springs, which are expected to have high-stress values, an enhanced nanostructured SS316L was selected. The properties of this material increased drastically compared to the base material after it was treated by thermal (austenitization and quenching) and hardening processes. The specific method of hardening employed is grain size refinement processes during an Equal Channel Angular Pressing (ECAP), showing a yield and ultimate strength of 1300 and 1340 MPa (Ueno et al. 2011). The specific chemical composition values and mechanical properties for each material are presented in Table 1 and Table 2.

Table 1. Chemical composition of the selected materials (Mohammad et al. 2012; Ueno et al. 2011)

Element (%)	C	Ni	Cr	Mn	P	S	Si	Mo	N	Fe
316L	0.02	11.21	17.38	1.86	0.027	0.0054	0.51	2.36	0.038	N/A
316L N	0.008	12.09	17.33	1.19	0.033	0.002	0.62	2.04	N/A	Balance

Table 2. Mechanical properties of the selected materials (Mohammad et al. 2012; Ueno et al. 2011)

Property	S_y [MPa]	S_{ULT} [MPa]	E [GPa]	Fatigue limit [MPa]	Poisson's ratio -
316L	332	673	165	146.45	0.3
316L N	1300	1340	195	570	0.3

2.3. Rules and Regulations

Regulations are required in the design and evaluation processes. In this study, standards established by the IMO (IGC Code) were followed to ensure the safety requirements and lifespan of the components. The regulations ICG code section 4.23 and DNV-RU-SHIP Pt.4 Ch.7 rule and the guide document DNV-CG-0135 were used in the process. The guidelines application can be identified in the design phase for scantling the components, and in the result evaluation in terms of allowed stresses in the tank and the expected fatigue life span.

2.3.1. Scantling

For the scantling definition, the parameter that should comply with the rules is the thickness of the elements exposed to internal pressure. The components of the LH2 storage unit exposed to internal pressure are the inner tank, composed of shells and ends, and the pipes connected to this tank. In the DNV-RU-SHIP Pt.4 Ch.7 Sec.4 [3.2], the minimum thickness for a cylindrical shell is retrieved from Equation (1).

$$s \geq \frac{p_c \cdot D_o}{20 \cdot \sigma_t \cdot v + p_c} + c \tag{1}$$

Where:

c : Corrosion margin. For stainless steel, this value is zero.

D_o : Outside diameter.

p_c : Calculating pressure. Corresponding to the LH2 evaporation.

s : Thickness.

v : Joint efficiency. For tanks storing LNG and similar, the value is one.

σ_t : Nominal design stress at calculating temperature.

In the same chapter of the DNV rule, DNV-RU-SHIP Pt.4 Ch.7, the expressions to dimension the thickness of the dished ends (section 4.1.1) and pipes (section 3.5.1) present a similar form but with a characteristic factor such as diameter or shape factor. Equation (2) corresponds to the dished ends. In this expression, β is the shape factor, which is a function of the outside diameter and outside height of curvature of the dished end. For computing the thickness of pipes, Equation (3) shows the factor d_o, which represents the outer diameter of the tube.

$$s \geq \frac{p_c \cdot D_o \cdot \beta}{20 \cdot \sigma_t \cdot v} + c \tag{2}$$

$$s \geq \frac{p_c \cdot d_o}{20 \cdot \sigma_t + p_c} + c \tag{3}$$

The reinforcements required due to openings in the inner tank are calculated using section 6.3 of the same chapter of the DNV rule, the expression is presented in Equation (4). The area calculated with this expression should be located on each side of the center line of the opening

as shown in Figure 5 and should be located at a distance L_s, see Equation (5), for the shell and L_b, see Equation (6), for the branch or attachment.

$$A_r \geq k \left(\frac{d_i}{2} + s_b \right) s_s \tag{4}$$

$$L_s = \sqrt{(D_i + s_{sa})s_{sa}} \tag{5}$$

$$L_b = 0.8 \sqrt{(d_i + s_{ba})s_{ba}} \tag{6}$$

Where:

A_r : Reinforced area

k : Calculation factor. For spherical shells, the value is one.

d_i : Internal diameter of the opening or branch.

s_b : Thickness of the attached pipe or branch.

s_s : Thickness of the shell.

D_i : Internal diameter of the shell.

s_{sa} : Thickness of the shell minus the corrosion allowance.

s_{ba} : Thickness of the branch minus the corrosion allowance.
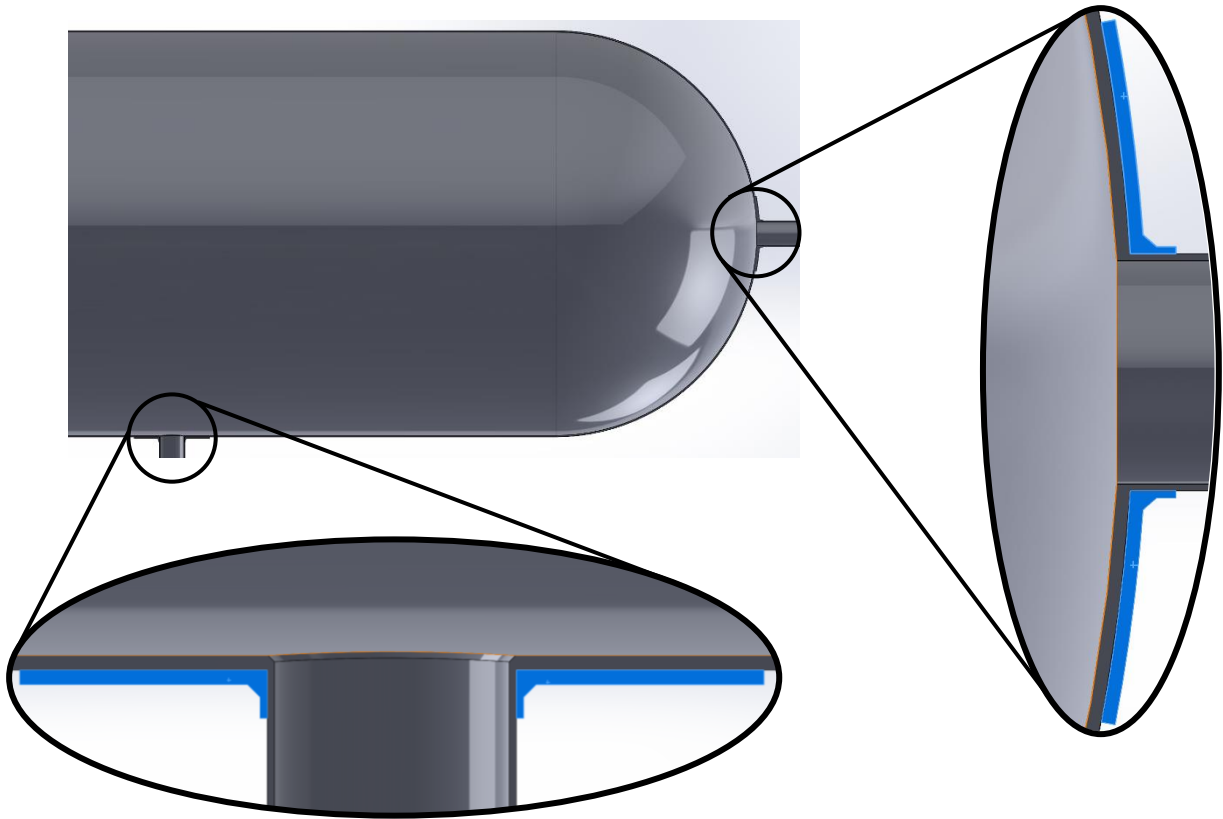
Figure 5. Opening reinforcements distribution

It is important to note that for elements subjected to internal pressure, a minimum thickness is specified as a function of the construction material for large components such as tanks, boilers, and large pipes. For small tubes, the external diameter is used as a reference to set the minimum allowed thickness. That value should be selected in scenarios when the computed thickness is less than this limit. For instance, the minimum thickness of shell components for carbon-manganese steels and nickel steels shall not be less than 5 mm, this value is set as 3 mm for austenitic steels and 7 mm for aluminum alloys. For tubes bearing internal pressure, this value ranges from 1.75 mm for an outside diameter of 38 mm or less to 3.5 mm for external diameters between 102 - 127 mm.

2.3.2. Allowable Stresses

In the regulations for storage tanks carrying liquefied gases at low temperatures, stress limits are set to guarantee the integrity of the storage unit components. In the ICG code, the values of these limits are defined as factors of the parameter f. This parameter corresponds to the minimum value between the yield or the ultimate strength with a constant related to the construction material as shown in Equation (7).

$$f = min\left\{\frac{R_m}{A}; \frac{R_e}{B}\right\} \tag{7}$$

Where:

f : Allowable stress parameter.

R_m : Tensile strength at room temperature.

R_e : Yield stress at room temperature.

A : Tensile strength material dependent coefficient:

$A = 3$; for nickel steels and carbon-manganese steels

$A = 3.5$; for austenitic steels

$A = 4$; for aluminum alloys

B : Yield strength material dependent coefficient:

$B = 1.5$; for nickel steels and carbon-manganese steels

$B = 1.5$; for austenitic steels

$B = 1.5$; for aluminum alloys

Once reference parameter is defined, limit stress values are determined from the expressions displayed in Equations (8) to (14). Considering these limits, the tank's compliance with international standards can be evaluated by comparing the stress values obtained from the numerical simulations with the established values from these equations. These stress limits specified by the IGC code apply to the tank exposed to internal pressure. In the case of this study, it applies to the inner tank of the LH2 storage unit where the fuel will be stored.

$$\sigma_m \leq f \tag{8}$$

$$\sigma_L \leq 1.5f \tag{9}$$

$$\sigma_b \leq 1.5f \tag{10}$$

$$\sigma_L + \sigma_b \leq 1.5f \tag{11}$$

$$\sigma_m + \sigma_b \leq 1.5f \tag{12}$$

$$\sigma_m + \sigma_b + \sigma_g \leq 3f \tag{13}$$

$$\sigma_L + \sigma_b + \sigma_g \leq 3f \tag{14}$$

Where:

σ_m : Equivalent primary general membrane stress

σ_L : Equivalent primary local membrane stress

σ_b : Equivalent primary bending stress

σ_g : Equivalent secondary stress

2.3.3. Accelerations

Accelerations generated by the ship's movement during the transportation process due to the operational conditions are transmitted to the tank structure inducing loads. According to regulations such as DNV rules, the accelerations induced by the six degrees of freedom of the ship can be combined into longitudinal, transversal, and vertical accelerations by empirical equations. In the rule DNV-RU-SHIP Pt.3 Ch.4, it is specified that for machinery installed at any position, the envelop accelerations are required and correspond to the maximum design values. In Equations (15) to (17), the expressions to compute the longitudinal, transverse, and vertical accelerations are presented in that order.

$$a_x = 0.7f_L \left(0.65 + \frac{2z}{7T_{SC}} \right) \sqrt{a_{surge}^2 + \frac{L_0}{325} \left[g \sin \varphi + a_{pitch-x} \right]^2} \tag{15}$$

$$a_y = \left(1 - e^{-\frac{B \cdot L}{215GM}} \right) \sqrt{a_{sway}^2 + \left(g \sin \theta + a_{roll-y} \right)^2} \tag{16}$$

$$a_z = \sqrt{a_{heave}^2 + \left[\left(0.95 + e^{-\frac{L}{15}}\right)a_{pitch-z}\right]^2 + (1.2a_{roll-z})^2} \qquad (17)$$

Where:

a_x	:	Longitudinal acceleration
a_y	:	Transverse acceleration
a_z	:	Vertical acceleration
f_L	:	Length dependent factor
z	:	Vertical distance from the center of gravity
L_0	:	Longitudinal distance from the center of gravity
T_{SC}	:	Scantling draught
B	:	Beam
L	:	Length
GM	:	Metacentric height
a_{surge}	:	Acceleration in surge direction
a_{sway}	:	Acceleration in sway direction
a_{heave}	:	Acceleration in heave direction
$a_{pitch-x}$	:	Longitudinal acceleration due to pitch
$a_{pitch-z}$	:	Vertical acceleration due to pitch
a_{roll-y}	:	Transverse acceleration due to roll
a_{roll-z}	:	Vertical acceleration due to roll
g	:	Gravity
φ	:	Pitch angle
θ	:	Roll angle

2.3.4. Fatigue Life

According to the IMO (IGC Code), the functional requirement for the design life of a storage tank installed on a ship must be in agreement with the design life of the vessel. Depending on the ship type, the design life span can range between 20 to 30 years, and it is mainly influenced by operational loads and environmental loads. For an LH2 storage tank on board, both load types are identified as affecting its fatigue endurance. The first loading type corresponds to the

ship's motion response to the sea state in any of the possible ship's movements heave, roll, surge, yaw, pitch, and sway directions, or combinations thereof, as explained in the previous section. Loads produced by this condition are introduced as accelerations in the vertical, transverse, and longitudinal components. The design life of the tank for this loading type should be not less than 10^8 as a probability of experiencing that acceleration value.

The second loading type is the loading and unloading processes of the tank during the bunkering scenario. Stresses generated by this process are related to the variation in temperature the tank and its components experience, plus the internal resulting pressure from evaporation of the LH2. For this loading type, the expected life span shall not be less than 10^3 filling cycles. This loading condition is considered to produce larger stresses in the structure if compared with the first scenario.

A complete fatigue life analysis must consider fatigue damage generated by both loading types over the tank (IGC Code). The cumulative fatigue damage (C_w) produced by these applied loads can be computed using the Equation (18). The damage produced by the ship's movement loading type is introduced in the expression by the factors n_i and N_i. The second fraction is associated with the bunkering loading type.

$$\sum \frac{n_i}{N_i} + \frac{n_{Loading}}{N_{Loading}} \leq C_w \tag{18}$$

Where:

C_w	:	Cumulative fatigue damage
n_i	:	Number of stress cycles related to the ship's movement scenario
N_i	:	Number of cycles before fracture for the stress amplitude related to the ship's movement scenario. Obtained from the FAT curves
$n_{Loading}$	:	Number of bunkering cycles during the lifespan. Bunkering scenario
$N_{Loading}$	:	Number of cycles before fracture for the stress amplitude related to the bunkering scenario. Obtained from the FAT curves

For the ship's movement loading case, the methodology to compute the number of cycles corresponds to the one explained by Young-IL Park (Park et al. 2021) and referred to the Korean Register of Shipping of the IGC code. This methodology uses Figure 6 and Equations (19) and (20) to calculate the number of cycles and the stress amplitude. Eight fatigue loads are defined to later derive the frequency of occurrence.
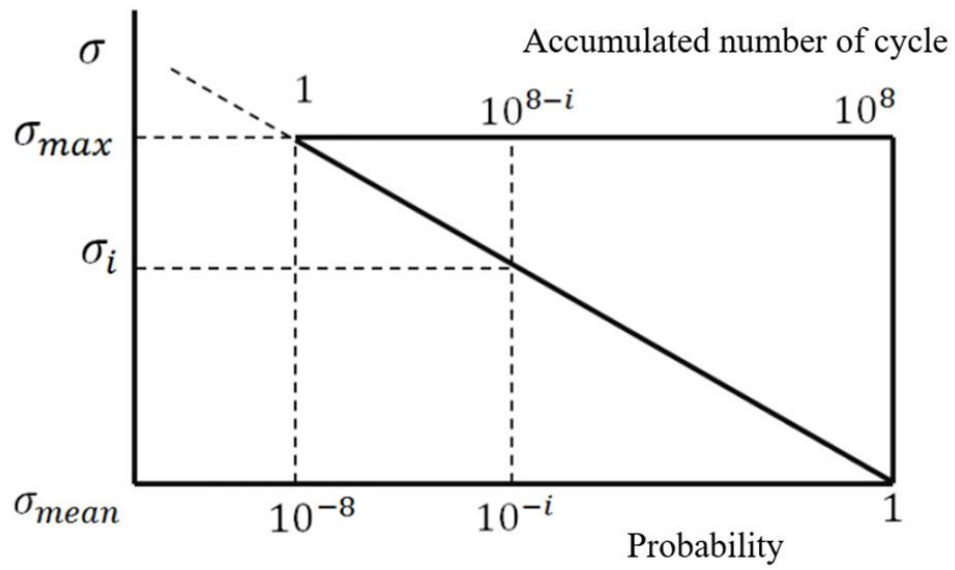
Figure 6. Calculation of fatigue stress and number of cycles (Park et al. 2021)

$$\sigma_i = \frac{17 - 2 \cdot i}{16} \cdot \sigma_{max} \qquad (19)$$

$$n_i = 0.9 \cdot 10^i \qquad (20)$$

3. NUMERICAL SIMULATIONS

This chapter covers the process used to perform numerical simulations of the LH2 storage tank model presented in the previous section. The software used to perform the different numerical simulations is ANSYS Workbench 2023 R1. Following the design and material selection, the FEA starts with the geometry preprocessing for mesh generation. Then, the tank model is meshed once the geometry is prepared, and mesh parameters are properly set. The next step is defining the boundary conditions for thermal and structural simulations. After this, a convergence study is performed to ensure results that are not mesh size dependent. This process helps identifying singularities and tuning up the mesh parameters. Finally, thermal and structural analyses are set up to retrieve stresses generated by thermal and structural loads. With these results, the postprocessing stage can be performed to determine the structural stresses as well as the fatigue life prediction.

3.1. Geometry of the Tank Model

The model presented in section 2.1 was imported as STEP files. Then, it was prepared using the SpaceClaim editor. In order to have better control of the mesh size, especially around the pipe connection in the tanks, the bodies of the inner and outer tanks were divided into 18 shells each as shown in Figure 7. Then, to ensure correct node coupling between these shells, shared topology was enabled for each tank. For all the other components of the storage unit, where shared topology was not enabled, linear connections were imposed to maintain the linearity in the simulations. Connection types implemented in the model will be further explained in the section 3.3 related to the loading conditions considered during the analyses.
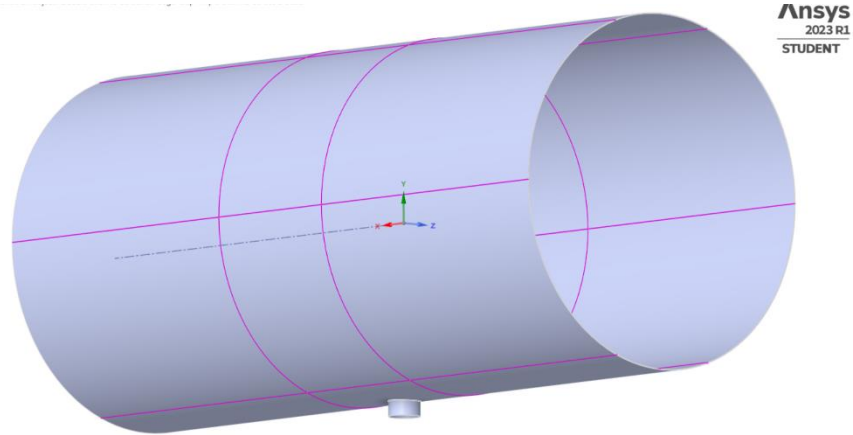
(a) Outer tank body
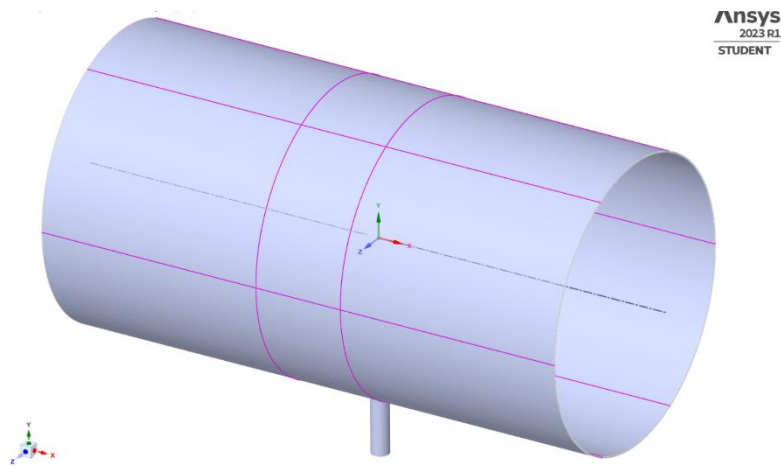
(b) Inner tank body

Figure 7. Division of both tanks' bodies into shells

An additional note regarding the tank model is how the springs were enumerated during the simulation process. As mentioned in the section 2.1, the spring arrangement is made up of four rows of four springs each as presented in Figure 8.
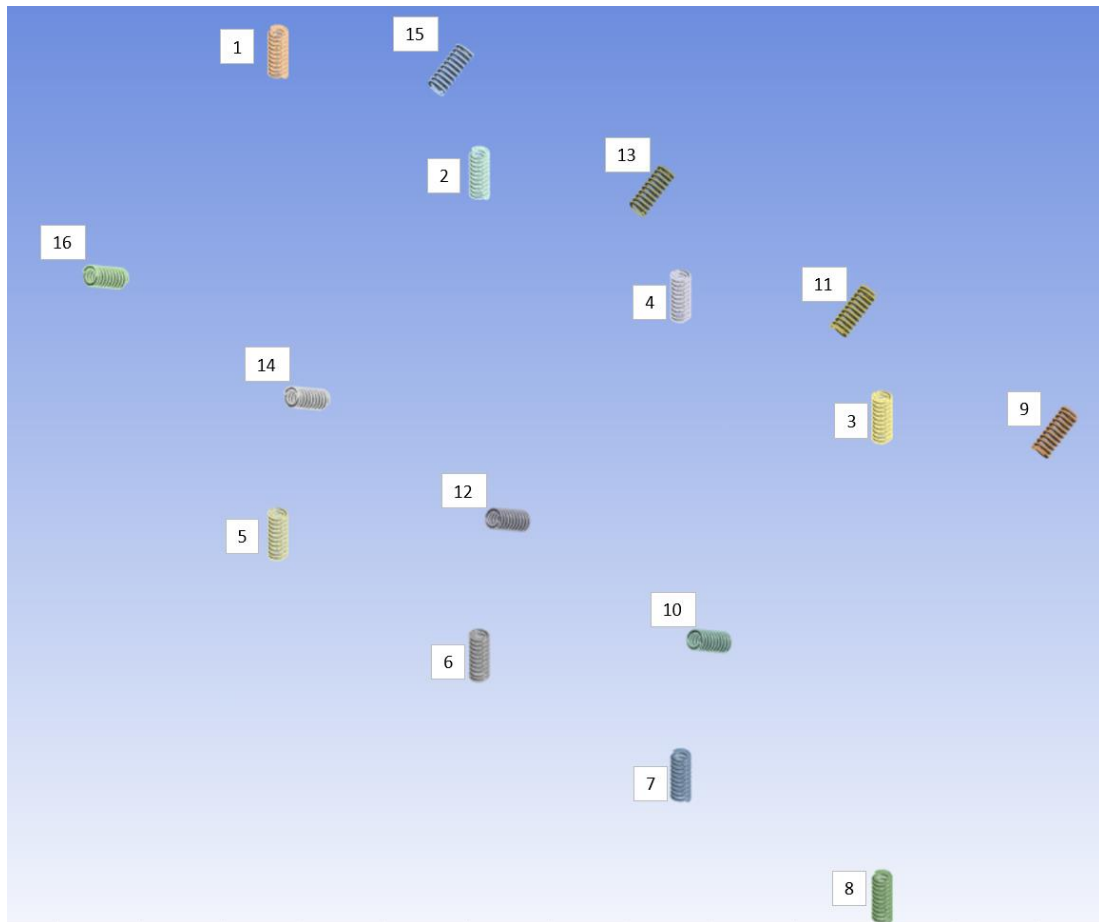
Figure 8. Springs arrangement numeration

3.1.1. Definition of the Springs for the Numerical Simulations

Springs can be defined using two approaches. The first one is using the spring connection option available in the connection's menu of the software. This built-in option creates a non-meshable spring between the selected elements saving computational power. Parameters more specific to the spring design such as spring constant, spring type, preload, damping, etc., need to be defined. Because of the impossibility of meshing the spring, the stress distribution in the spring cannot be retrieved in the numerical simulation. As the purpose of this study was to determine the performance of the spring connection between the tanks, this option was not selected.

The second option is modeling the springs in CAD software and considering them as any other component of the tank. This approach was adopted in this research. The geometry of the springs was imported into the Ansys program, along with the rest of the components of the storage unit. Within the program, the springs are defined as flexible and deformable elements. Material

properties such as tensile yield strength, ultimate strength, young modulus, and Poisson's ratio were specified (see Table 2). Then, the bonded connection was employed to connect each end of the springs to their corresponding inner and outer attachments. The bonded connection is explained in detail in the section 3.3.

3.2. Tank Dimensions

In the previous chapter, the tank design was introduced, and the discussion focused on explaining its components, disposition, and functionality. That section was intended to express the design purpose and to present the spring connection system as the innovative part of the design. In this section, the dimensions of tanks and springs are detailed in Table 3 and illustrated in Figure 9 and Figure 10. These parts, tanks and springs, of the LH2 storage unit are considered the most relevant for the analysis since high-stress values are expected due to the operational conditions.

Table 3. Dimensions of relevant storage unit components

| Element	Dimension	Parameter	Values	Units
Inner tank	Length seam to seam	L_{s1}	3638.60	[mm]
	Internal diameter	D_{o1}	1907.50	[mm]
	Thickness	S_1	7.00	[mm]
	Length including caps	L_{T1}	5546.10	[mm]
Outer tank	Length seam to seam	L_{s2}	5030.00	[mm]
	Internal diameter	D_{o2}	2321.50	[mm]
	Thickness	S_2	4.70	[mm]
	Length including caps	L_{T2}	5969.50	[mm]
Spring	Outer diameter	D_o	75.00	[mm]
	Inner diameter	D_1	51.00	[mm]
	Wire diameter	d	12.00	[mm]
	Mean diameter	D	63.00	[mm]
	Free length	L_f	200.00	[mm]
	Pitch	p	20.71	[mm]
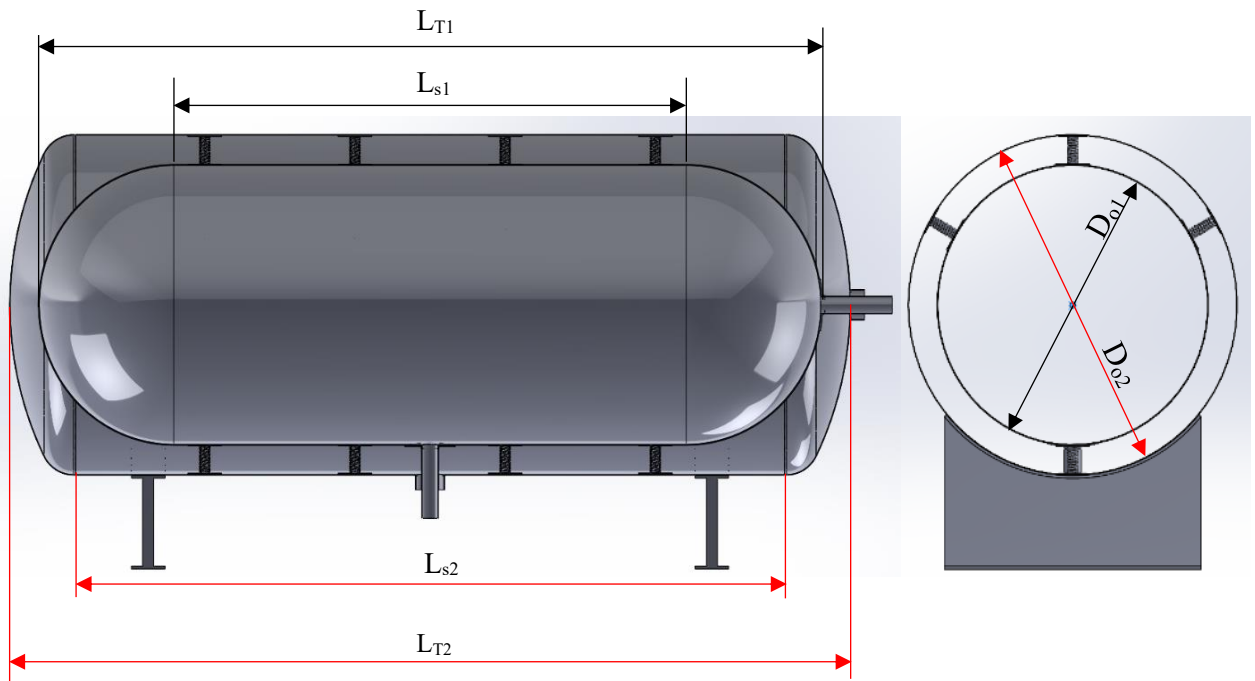
Figure 9. Tanks main dimensions
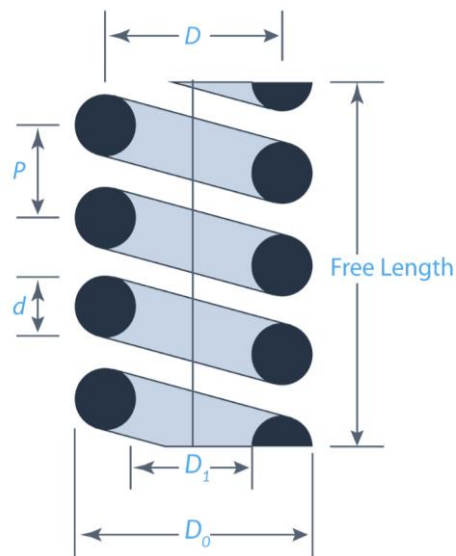
Figure 10. Springs main dimensions (EngineerExcel)

3.2.1. Mesh Generation

The mesh generation stage of the numerical simulation involves discretizing the geometry into finite elements by choosing the appropriate parameters to accurately simulate the behavior of the tank. The results can vary drastically if the mesh parameters are not tuned up properly, leading to mesh-dependent results. This effect is characterized by incorrect results or singularities where local nodal values, such as deformations or stresses, change drastically concerning the node's neighborhood. Aspects such as finite element order, mesh density, and meshing method are related to this effect and the convergence of the results. The selection process of the finite element order and meshing method are addressed in this section, while the mesh density is covered in the mesh convergence analysis in section 3.5.

Within the FEA, discretizing the geometry is achieved by dividing each component of the model into small domains where approximation functions, known as shape functions, are defined to determine nodal values. Shape functions are represented by polynomials of first or second order corresponding to linear and quadratic finite elements. The selection process between these two finite element types is governed by the required accuracy, geometry complexity, and available computational power. For applications such as the LH2 storage tank of this study that presents a complex geometry, large stress gradients, and demanding high accuracy; quadratic finite elements are desired.

The second important aspect that allows the creation of a high-quality mesh is constructing a well-structured arrangement of finite elements. This can be achieved by setting the meshing method for each component as a function of any characteristic geometrical aspect. For instance, revolved bodies, such as the cylindrical tank body, are preferred to be meshed by the sweep method or hexahedral elements. For complex designs, with attachments or irregular geometries where a structured mesh fails, tetrahedral and multizone methods are preferred. In scenarios where a specific element size or number of divisions in edges are needed, the sizing method can be applied. Some of these methods can be combined to improve the mesh quality. Considering the complexity of the storage unit, a combination of methods for some components was implemented. Table 4 shows a summary of the methods employed for each part of the assembly.

Table 4. Meshing method and element order for each component of the LH2 tank

Component	Element Order	Method
Springs	Quadratic	Sizing
Legs:		Multizone / Sizing
S1		Sizing
S2	Quadratic	Sizing
S3		Sizing
Inner tank ends	Quadratic	Sizing
Outer tank ends	Quadratic	Tetrahedrons
Inner plates	Quadratic	Sizing
Outer plates	Quadratic	Sizing
Inner tank:		-
Shells 1 (H)		Sweep / Sizing
Shells 2 (V)		Sweep / Sizing
Holes 1 (H)	Quadratic	Multizone / Sizing
Holes 2 (V)		Multizone / Sizing
Pipes		Sizing
Pipe_R		Multizone / Sizing
Outer tank:		-
Shells 1 (H)		Sweep / Sizing
Shells 2 (V)		Sweep / Sizing
Holes 1 (H)	Quadratic	Multizone / Sizing
Holes 2 (V)		Multizone / Sizing
Pipes		Sizing

Table 4 shows that components such as the legs were meshed with two meshing methods because of their complex geometry. The initial mesh was generated using the multizone method. Then, improvements in the mesh structure were achieved by applying the sizing meshing method along the set of edges S1, S2, and S3 as depicted in Figure 11.

(a) S1 edges

(b) S2 edges

(c) S3 edges
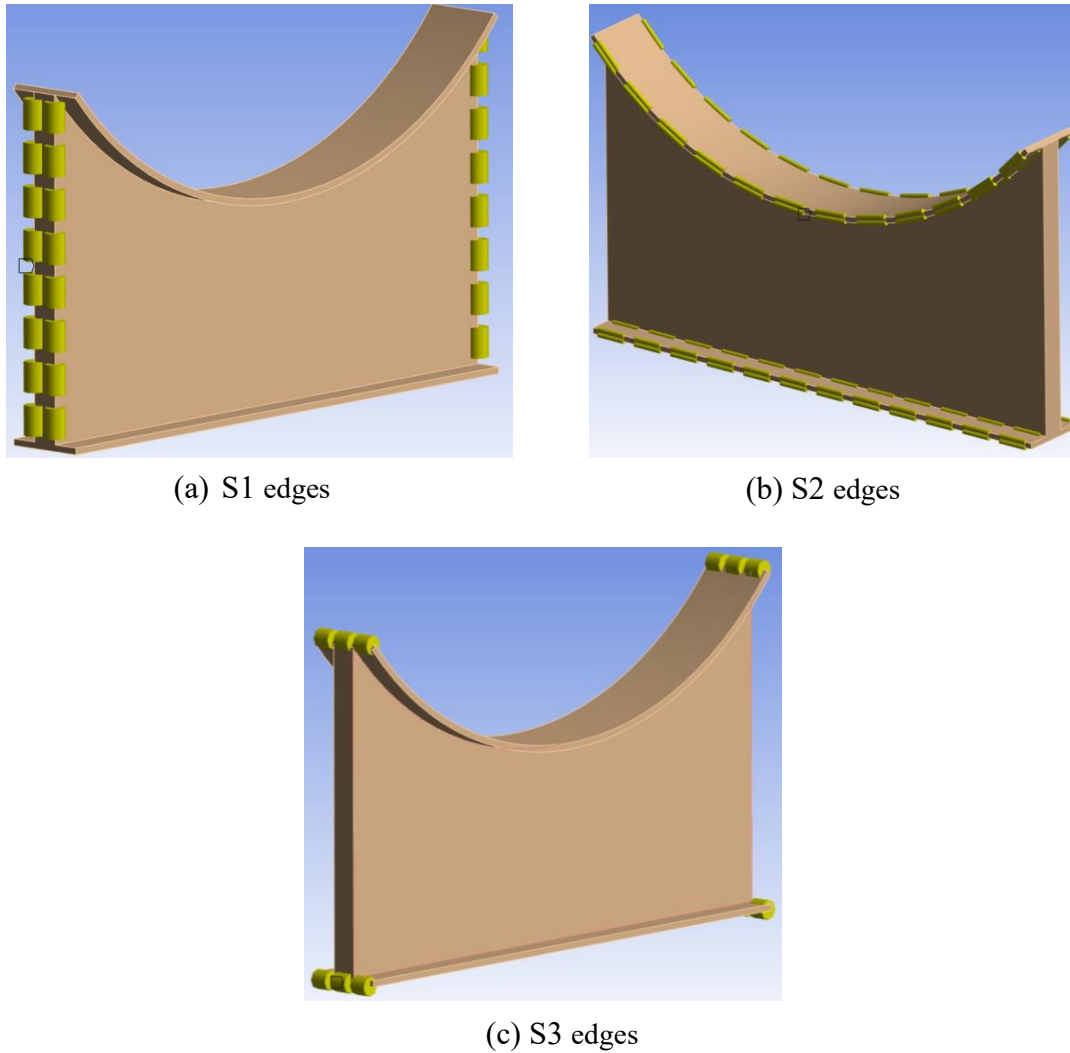
Figure 11. Legs meshing parameters

For components made up of multiple parts, such as cylindrical bodies of both tanks, various meshing methods were utilized. With this operation, more control was achieved over the element size around the shells with holes for the piping connection while having a smooth mesh size transition in the other shells. Depending on the type of shell, sweep or multizone method was employed for the initial mesh. Subsequently, the sizing method was used to improve the mesh structure. Parameters such as Shells 1 (H) and Shells 2 (V) represent the horizontal and vertical set of edges used in shells without holes, respectively. In the same way, Holes 1 (H) and Holes 2 (V) were implemented for the shells with holes. Additionally, the edges of the attached pipes and reinforcement due to openings in shells were meshed with the sizing method. These parameters are displayed in Figure 12 for normal shells and shells with holes. This configuration was implemented in both tanks. Figure 13 shows the meshing parameters for the attached pipes and their reinforcements.
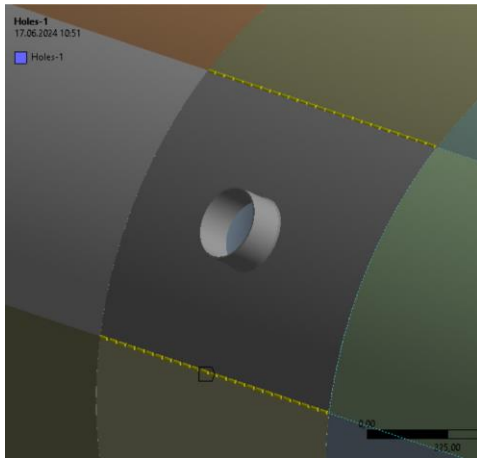
(a) Holes 1 (H)
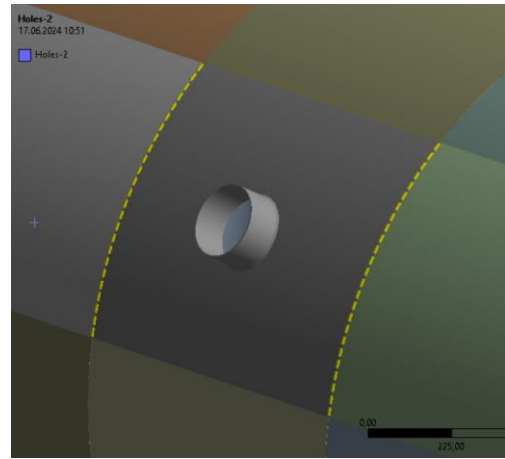
(b) Holes 2 (V)
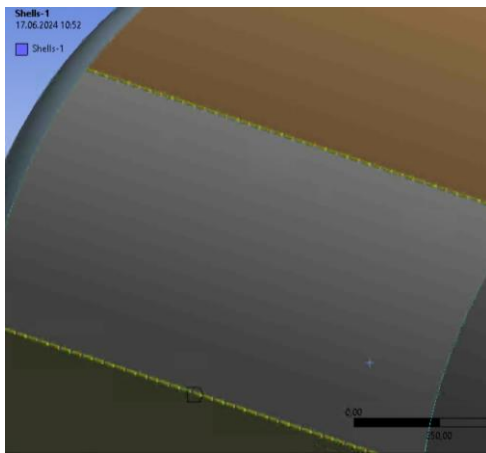
(c) Shells 1 (H)

(d) Shells 2 (V)

Figure 12. Tanks meshing parameters
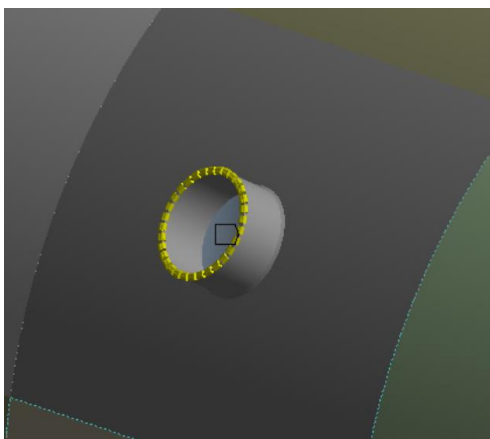
(a) Pipe
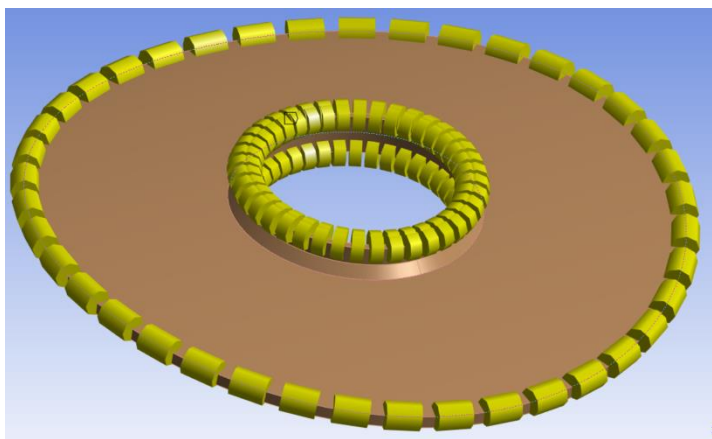
(b) Pipe_R

Figure 13. Pipe and pipe reinforcement meshing parameters

3.3. Loading Conditions

Following the numerical simulation workflow, the problem's loading and boundary conditions are defined for the thermal and structural analyses. Boundary conditions are constraints represented mathematically in a numerical simulation that captures the interactions of the studied object with the environment. Defining both, loading and boundary conditions is a crucial step in the FEA as the results can drastically change depending on this process. Essential and natural boundary conditions were set for the structural and thermal simulations. Before defining specific load conditions of each simulation, constraints related to the structure itself were established. These essential constraints are the connections between distinct parts of the assembly and were implemented in all the simulations.

As mentioned in the section 3.1, shared topology option was employed to connect the shells of the cylindrical body of each tank. This option ensures that nodes located at the interfaces between shells are shared keeping linearity in the simulation. As a benefit of it, the mesh is continuous through all the elements connected with this option, and nodal values are transferred from one to the next element. Required computational power is reduced for elements linked with this method since it does not impose constraints on the model. All other components of the LH2 storage tank were joined using linear constraining connections.

Among the connection types available in the program, there are two connections with linear definition: bonded and no separation connections. For elements intended to work as a single unit, such as those that are welded in reality, a bonded connection must be selected. This connection type restraints sliding, separation, and penetration between elements while ensuring that nodal values are transmitted linearly from one element to the next. The bonded connection enforces constraining equations on the nodes located at the interface between components. Unlike the shared topology option, the bonded connection does not connect node by node. Rather, it imposes the nodal values computed in the contact element to the target element.

The bonded connection type is often preferred over the shared topology function when dissimilar materials are defined in the touching parts, or if the mesh type and size differ considerably from two attached elements making it difficult to properly fit all the nodes from one to the other component. Although both connecting methods are similar, bonded connections tend to increase the number of equations that need to be solved, thereby more computational power is required to solve the problem. However, a key advantage of the bonded connection

31

compared to the shared topology is better control over mesh differences between connected components. This control is particularly useful when high stresses are expected in one of the components so that mesh refinement can be performed in that element.

The last loading condition defined in the model is a distributed mass of 1076.92 kg corresponding to the mass of the LH2 stored in the inner tank. The mass was applied along the internal surface of this tank as displayed in Figure 14.
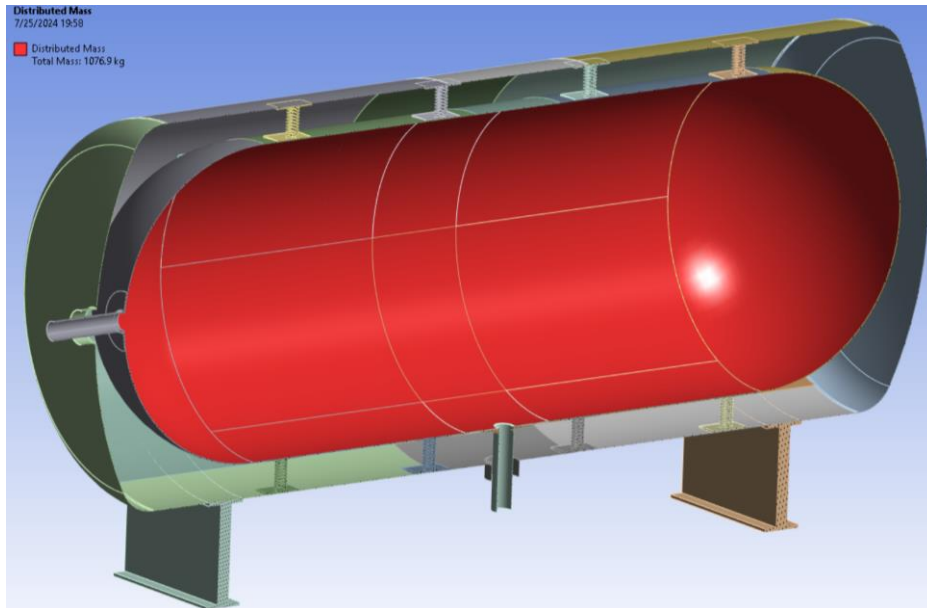
Figure 14. LH2 distributed mass applied in the inner tank

3.3.1. *Thermal Boundary Conditions*

Thermal simulation is intended to find the thermal distribution produced by the heat transfer from the environment to the inner tank. The necessary parameters to perform this simulation correspond to the operational conditions, tank design, and material. With the information from these three aspects, essential and natural boundary conditions can be defined. For this study, essential boundary conditions were set by the operational regimen of the tank, while natural boundary conditions were related to the design and selected material.

Two essential boundary conditions were defined for steady-state thermal simulation. The first imposed value is -255°C, assigned in the internal faces of the inner tank (see Figure 15), and corresponds to the LH2 storing temperature. The thermal condition is assumed uniform along the surface of the internal tank, which indicates the tank is already filled with LH2. The second

32

temperature, 5°C, associated with the surrounding environment is specified in the 'Initial Temperature' section.
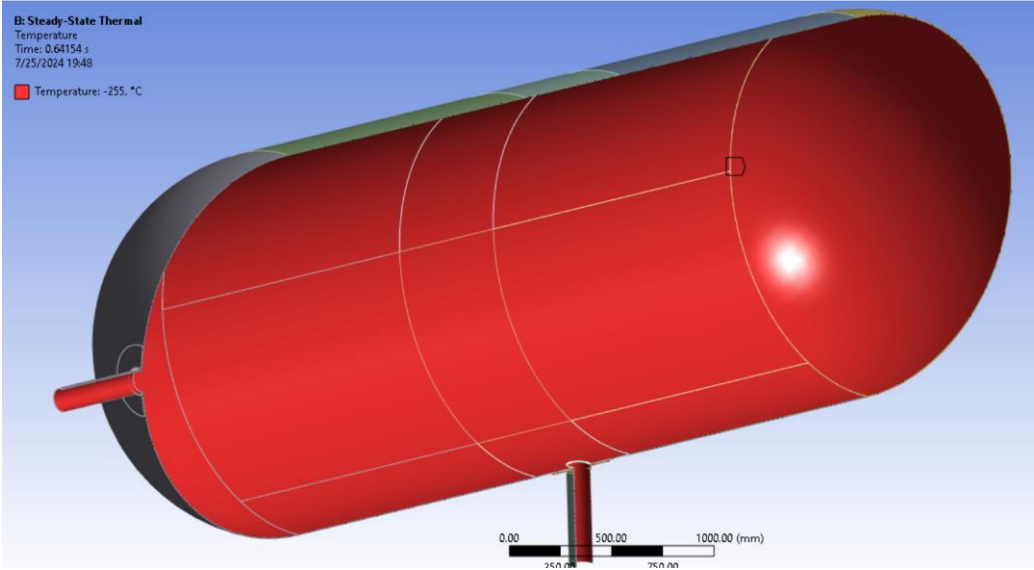
Figure 15. Inner tank temperature

The natural boundary conditions implemented are the heat transfer mechanisms present in the model. This set of impositions depends on factors such as thermal conductivity, emissivity, insulation methods between tanks, and so on. In the design, a vacuum is maintained in the space between the inner and outer tanks as an insulation medium. Taking advantage of it, convection is not considered in the analysis. Heat transfer by conduction is possible only through the spring connection and is defined by the material thermal conductivity property. For the stainless steel 316L selected, the value is 14.58 W/mC (Ansys 2023). Finally, radiation was set in the internal surface of both tanks with an emissivity value of 0.8 (Balat-Pichelin et al. 2022), as displayed in Figure 16.
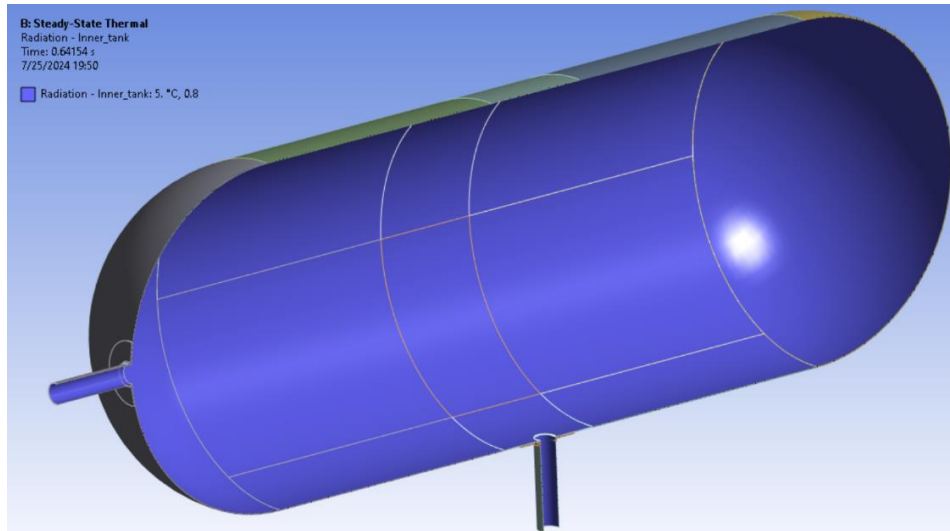
(a) Inner tank
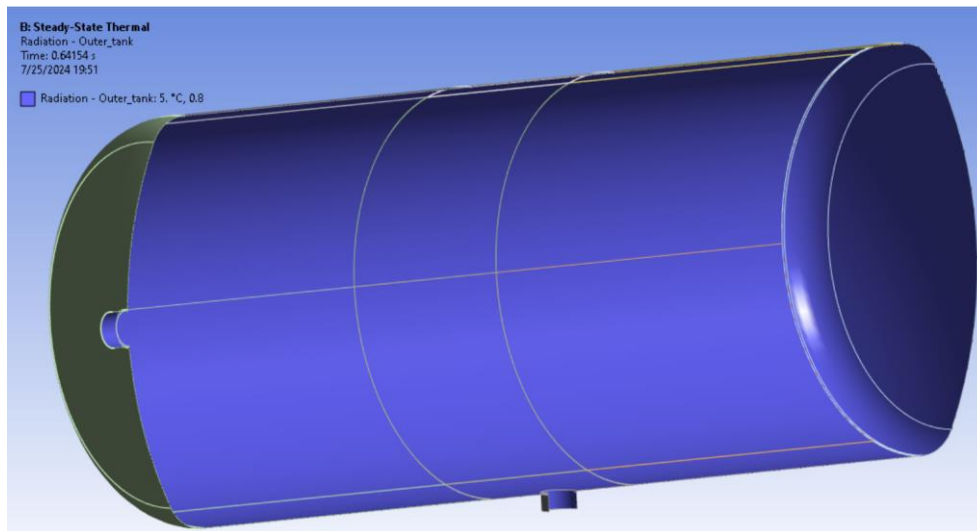
(b) Outer tank

Figure 16. Radiation boundary conditions defined in the tanks

3.3.2. Structural Boundary Conditions

Similar to the thermal case, structural boundary conditions can be classified into essential and natural types. Boundary conditions for the structural analyses are defined by different enforced restrictions in displacement, accelerations, and internal pressure present in the model. The essential boundary conditions applied to the model restrict all three translational displacements and three rotational degrees of freedom in the x, y, and z directions by setting them to zero. This fixed condition is applied in the legs of the LH2 storage unit as shown in Figure 17. This and

the boundary conditions related to the bonded connections defined before for the assembly are all essential boundary conditions considered for the structural simulations.
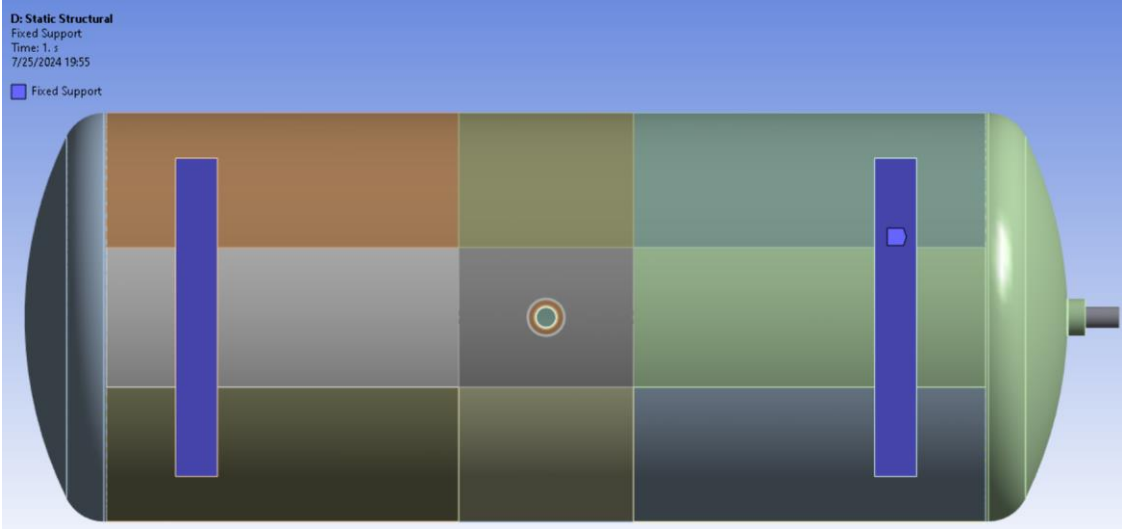
Figure 17. Legs fixed support boundary condition

Regarding the natural boundary conditions, gravity and accelerations in longitudinal, transverse, and vertical directions resulting from the ship's operational conditions were applied. These accelerations correspond to maximum design values, also known as envelope accelerations, specified in DNV-RU-SHIP Pt.3 Ch.4. The calculation process used the Equations (15) to (17), the information of the ship where the tank will be placed, and the position considering the ship's center of gravity. The data and the acceleration values are presented in Table 5. The last loading condition considered in the model is the pressure inside the inner tank produced by the evaporation of the LH2 due to heat transfer from the exterior. This value was set to 0.45 MPa and defined in the internal surface of the inner tank as shown in Figure 18.

Table 5. Ship's information, tank position, and acceleration values

Parameter	Value	Unit
Ship name	MOL Triumph	-
Length	400	[m]
Beam	58.8	[m]
Draft	16	[m]
Depth	32.8	[m]
Speed	22	[kt]
DWT	192672	[t]
Position of the tank		
Longitudinal	50	[m]
Transverse	0	[m]
Vertical	0.5	[m]
Accelerations		
Longitudinal	2.3	[m/s^2]
Transverse	2.2	[m/s^2]
Vertical	3.6	[m/s^2]
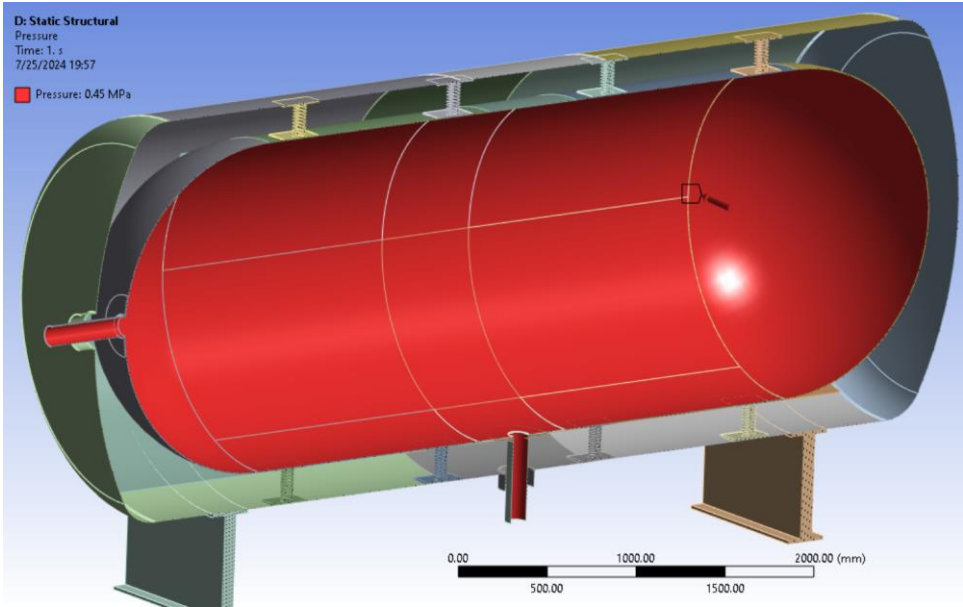
Figure 18. Pressure boundary condition in the inner tank

An additional classification that can be made for this model is general and specific loading case boundary conditions. The general boundary conditions implemented in the model include gravity, bonded contacts to connect all the parts, and a fixed condition applied to the legs of the

storage unit. Boundary conditions related to each specific loading case are divided into the cycling loads experienced by the tank. The LH2 storage tank will be exposed to the bunkering process and the ship's movement loading conditions. The imposition for the bunkering loading scenario in the structural numerical analysis is the pressure inside the inner tank. Accelerations are the loading conditions related to the ship's movement loading case.

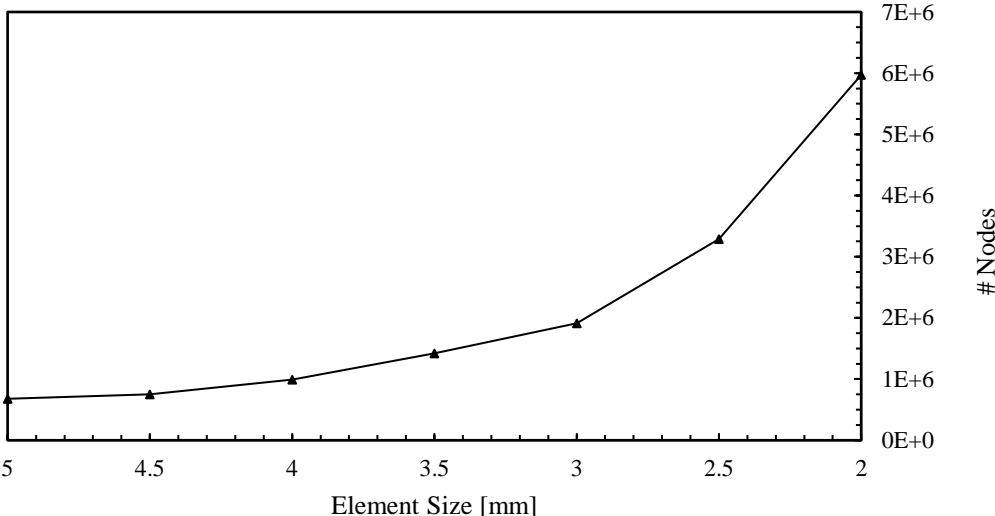## 3.4. Mesh Convergence

As discussed in section 3.2.1, the process of getting accurate results that are not dependent on the mesh density is called mesh convergence. This process was performed in two steps considering the bunkering loading condition. The first step was characterized by running an initial simulation implementing a coarse mesh to identify points where high-stress values are located. Once the general stress distribution on each component of the assembly is obtained, improvements in the mesh of parts with no critical points are performed. Components such as legs, connecting plates at both ends of the springs, and end caps of inner and outer tanks were identified in this group. Then, it is reviewed if those components experiment with stress variations, or if mesh refinement in these components influences the stress values of the parts presenting critical points. As a benefit of this, it was possible to identify the reference components to evaluate the convergence of the model. The components assigned to this group are the springs and the cylindrical body of both tanks. The springs were identified as the crucial parts of the convergence analysis because of their higher stress value compared to the tanks' bodies.

The second step of the process is the convergence analysis of the critical elements, in this case, the springs. A mesh size coherent with the other components' dimensions was set ensuring a good compromise between accuracy and computational power. Limitations in the size of these non-critical components allowed using a finer mesh in the springs. The convergence process started with a mesh size of 5 mm for the springs and refined until 2 mm using reductions of 0.5 mm. Another reason is that the stress values obtained for 3.0 and 3.5 mm show reasonable and stable values among other mesh sizes. Mesh variations of 0.1 mm were used to check the convergence around the limit size of 3 mm. For smaller mesh sizes, the simulation requirements of computational resources increase drastically which can be explained by the large increment

in the total number of elements and nodes of the model for mesh sizes smaller than 3 mm, as depicted in Figure 19.

(a) Number of nodes
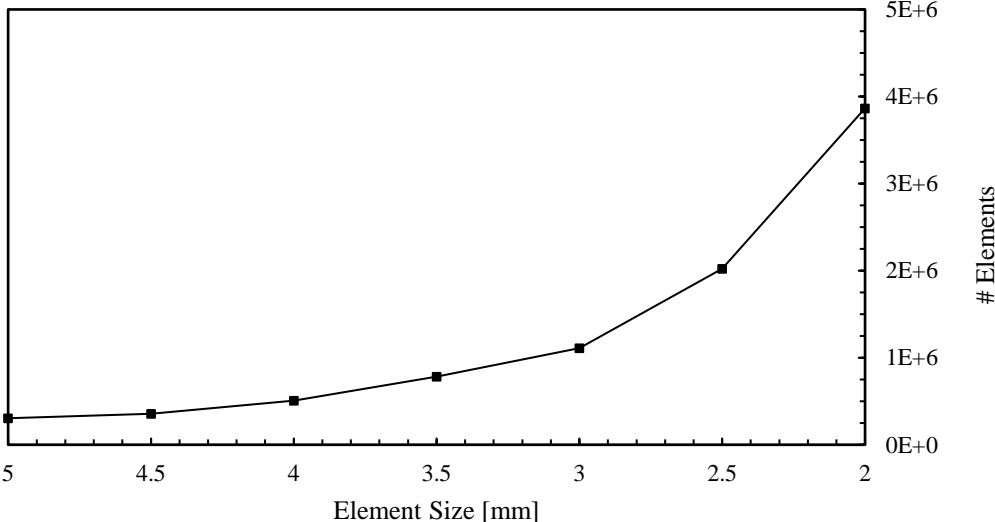
(b) Number of elements

Figure 19. Number of nodes and elements as functions of the spring mesh size

The convergence was analyzed using the data of the simulations with mesh sizes from 3.5 mm to 3 mm with size variations of 0.1 mm. The maximum von Mises equivalent stress of each spring was used to see the effect of the mesh refinement in the results of the numerical simulations. Three groups were defined according to the disposition of the springs in the tank to analyze the results. The first group consists of eight springs aligned vertically, with four at the top and four at the bottom of the inner tank. Figure 20 shows the results of this spring group. From this group, springs 3 and 4 present the highest stress values regardless of the mesh size. For the finest mesh, these two springs present a stress value of around 800 and 900 MPa. Also,

they show more stress variation with the changes in the mesh size compared to the others springs in this group. For all the other springs of this group, the stress variation is less and they converge into stress values ranging from 500 to 600 MPa.
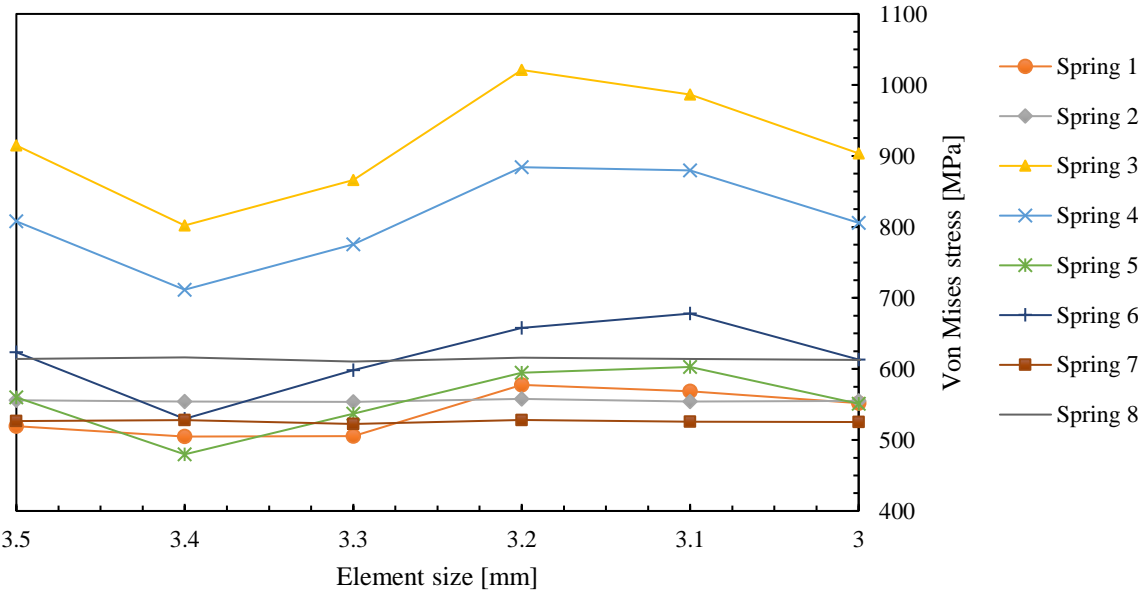
Figure 20. Stress vs. mesh size for springs 1 to 8

The second group is formed by the springs located at the back side of the LH2 storage tank as shown in the spring configuration isometric view in Figure 8. These springs are numbered with odd numbers from 9 to 15 and Figure 21 displays the plot of stress as a function of the mesh size for each of these springs. This group of springs is placed at an angle of 60° from the vertical and presents a similar variation behavior of springs 3 and 4 related to the mesh size variation. In this group, springs 9 and 11 experienced the highest stress values of the group with values of 926 and 850 MPa, respectively.
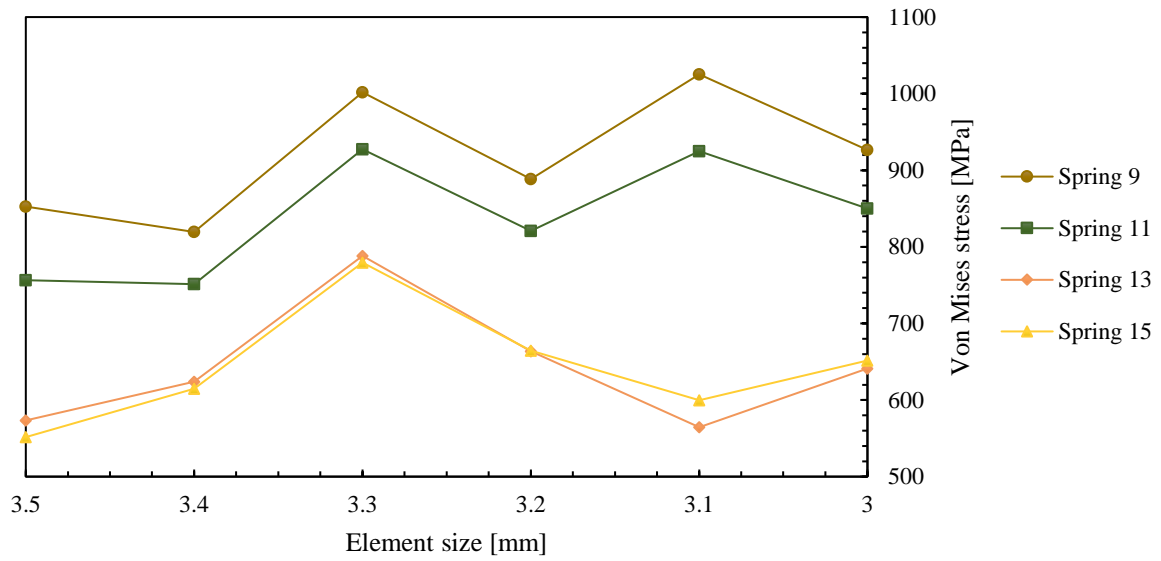
Figure 21. Stress vs. mesh size for springs 9 to 15 (odds)

Results of the mesh convergence analysis for the last spring group made up of springs numbered with evens from 10 to 16 are presented in Figure 22. These springs are located at the front part of the tank in the same angle disposition as the previous group. The stress values corresponding to the last three mesh size variations show a convergent trend to values around 900 and 830 MPa for springs 10 and 12. For springs 14 and 16, this value is 575 MPa.
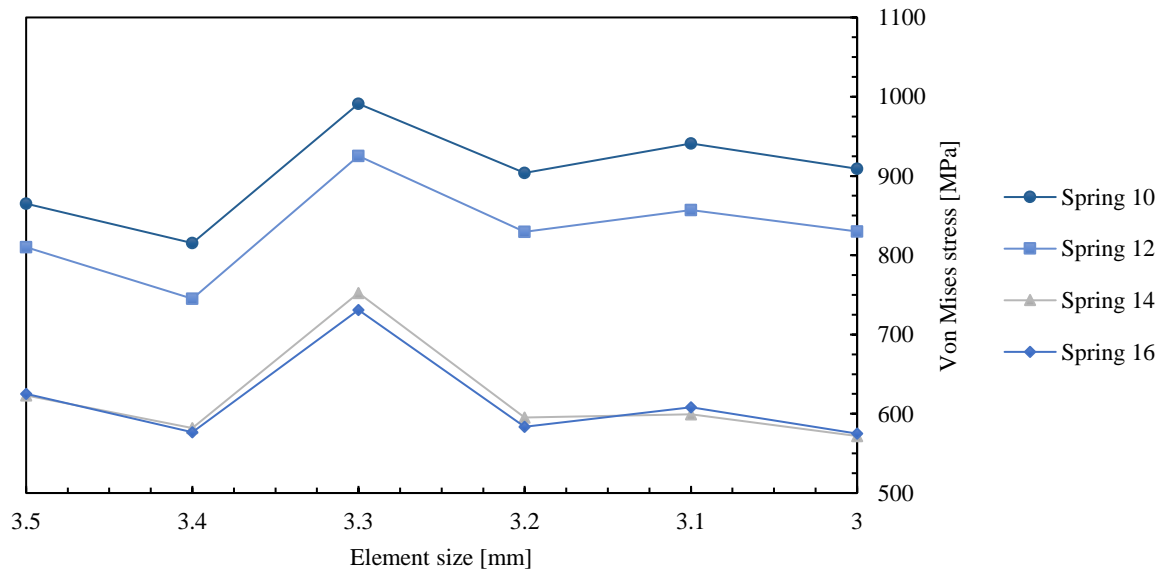
Figure 22. Stress vs. mesh size for springs 10 to 16 (evens)

In general, springs in groups two and three, and springs 3 and 4 of the first group show stress variations that might suggest the model is not fully converging into the real value in those springs with the finest mesh size used. Finally, Table 6 summarizes the mesh size employed for each component for the final mesh used in the numerical simulations. The total number of nodes and finite elements of the model is presented in this table. For the components where the number of divisions option was implemented in the mesh sizing method, the size of the finite elements was computed using the length of the edge where the divisions were imposed.

Table 6. List of the mesh size for each component of the LH2 storage unit

Component	Number of divisions	Size of elements [mm]	Dimension [mm]
Springs	-	3	-
Legs:			
S1	8	127.93	1023.46
S2	12	151.35	1816.21
S3	3	80.00	240
Inner tank ends	-	80	-
Outer tank ends	-	120	-
Inner plates	-	40	-
Outer plates	-	40	-
Inner tank:			
Shells 1 (H)	30	50.64	1519.30
Shells 2 (V)	22	49.54	1089.94
Holes 1 (H)	19	31.58	600.00
Holes 2 (V)	25	33.54	838.41
Pipes	12	31.42	376.99
Pipe_R	40	28.22	1128.78
Outer tank:			
Shells 1 (H)	20	100.75	2015.00
Shells 2 (V)	14	101.70	1423.87
Holes 1 (H)	25	40.00	1000.00
Holes 2 (V)	25	32.55	813.64
Pipes	32	20.56	657.85
Number of nodes		1911380	
Number of elements		1111743	

3.5. Thermal Analysis

Within the bunkering process, two loading conditions are identified which induce stresses in the storage unit. The first one is the thermal gradient along the components of the tank due to the large difference in the temperatures between the inner tank and the outer tank. The second condition is the pressure inside the inner tank. Stresses generated by the first load will be addressed in this section. The workflow to find these stresses in the tank produced by temperature-related operational conditions requires two numerical analyses. For the first one, a steady-state thermal analysis type was selected to perform the thermal analysis. The second analysis carried out is a static structural simulation.

3.5.1. Temperature Distribution

From the steady-state thermal simulation, the temperature distribution of the LH2 storage tank was retrieved, as shown in Figure 23. Considering that conduction and radiation heat transfer mechanisms were implemented in the model. It can be noted that the conduction mechanism through the springs is dominant in the model. It can be noted that spring elements are experiencing a large thermal gradient along their length of 200 mm. They present temperature values of 5°C in the end connected to the outer tank and -255°C in the end connected to the inner tank. This applied condition in the springs turns them into critical elements where high thermal stresses will be expected.
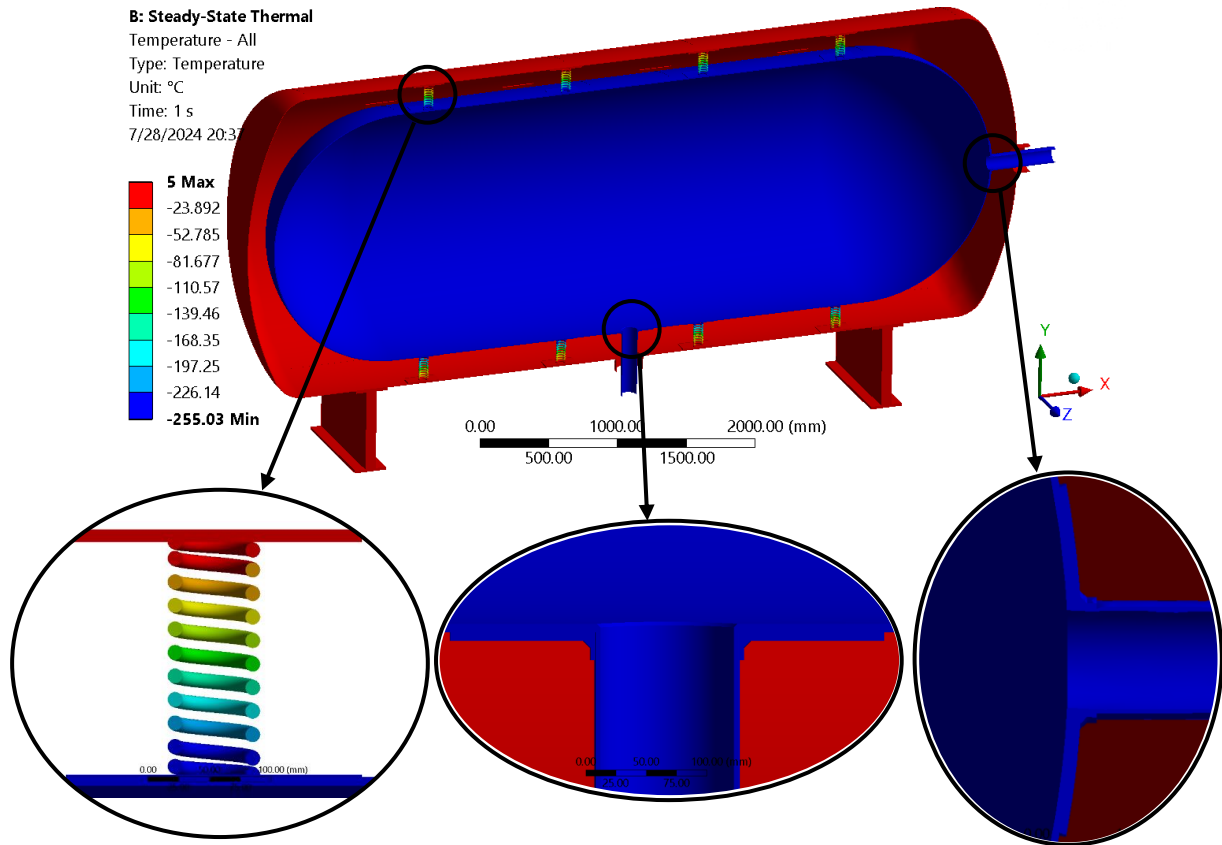
Figure 23. Temperature distribution of the storage tank

Figure 24 and Figure 25 present the temperature distribution of the outer and inner tanks. Isolating these components was necessary to show how the temperature has small variations at the points where the springs are connected. The outer tank presents a larger zone where the temperature varies compared to the inner tank. Additionally, these zones exhibit a well-defined circular shape, with the maximum temperature drop occurring at the center of each area. In contrast, the inner tank shows a diffuse zone, characterized by spots surrounding a point of maximum temperature increase. Within these zones, the maximum temperature variations are observed as a temperature drop of 0.63°C in the outer tank and a temperature rise of 0.1°C in the inner tank. Considering that the temperature variation in the outer tank is six times larger than in the inner tank, thermal stresses are expected to be higher in the outer tank.
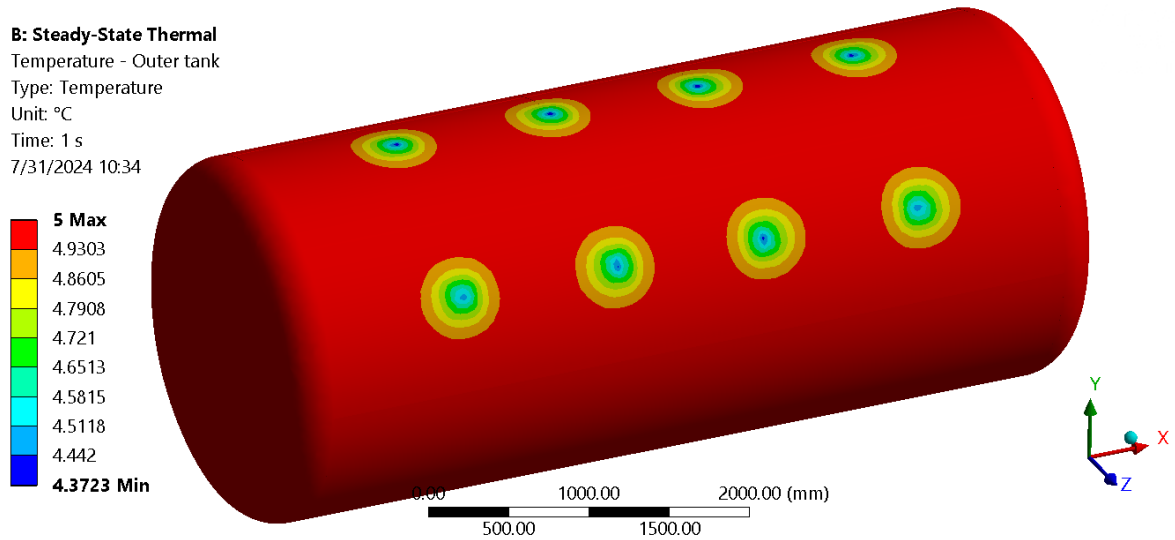
Figure 24. Temperature distribution in the outer tank
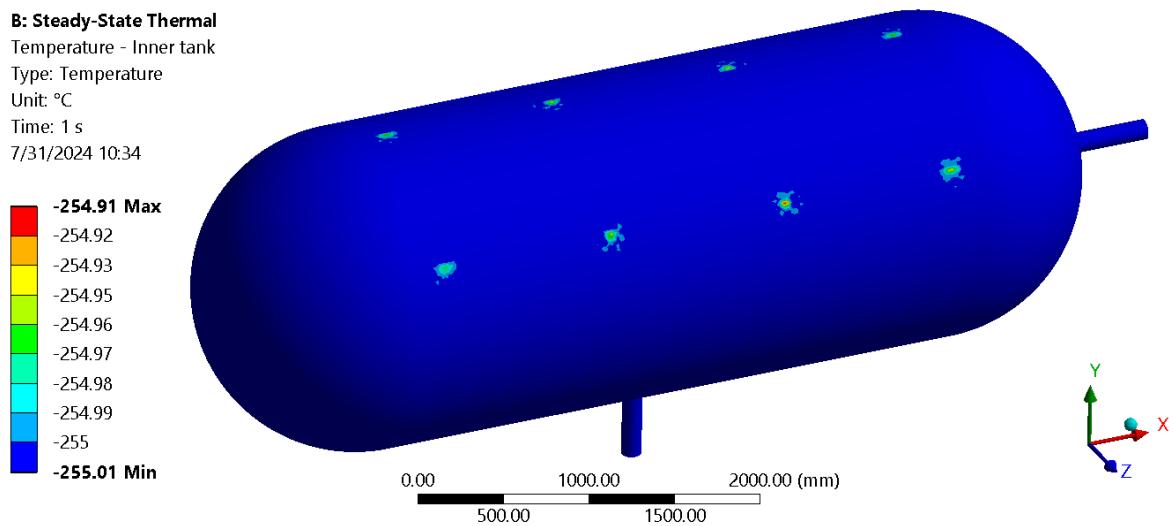
Figure 25. Temperature distribution in the inner tank

3.5.2. Thermal Stresses

Once the temperature distribution in the LH2 storage tank is obtained, the next step is to employ this information in a structural numerical analysis. This simulation uses the temperature distribution results as loading input. As observed in the temperature distribution in the previous section, the temperature is not constant along the extension of each component. With this data,

the stresses generated by the thermal expansion or contraction of the material depending on the temperature gradient present in each tank's component were computed.

The stress distribution of the outer tank is presented in Figure 26. It can be noted that stress values are located in the points where the springs are connected, especially at the bottom of the tank where the legs of the tank are located. High stress values can be identified in two zones of the bottom part of the tank. The first stress zone is around the legs and is caused by the constraints imposed by the rigidity of the legs. This rigidity prevents the free movement associated with the thermal expansion or contraction of the tank, leading to increased stress values in this area. The second zone, where the maximum stress value is located, is in the geometry change corresponding to the pipe connection edge.
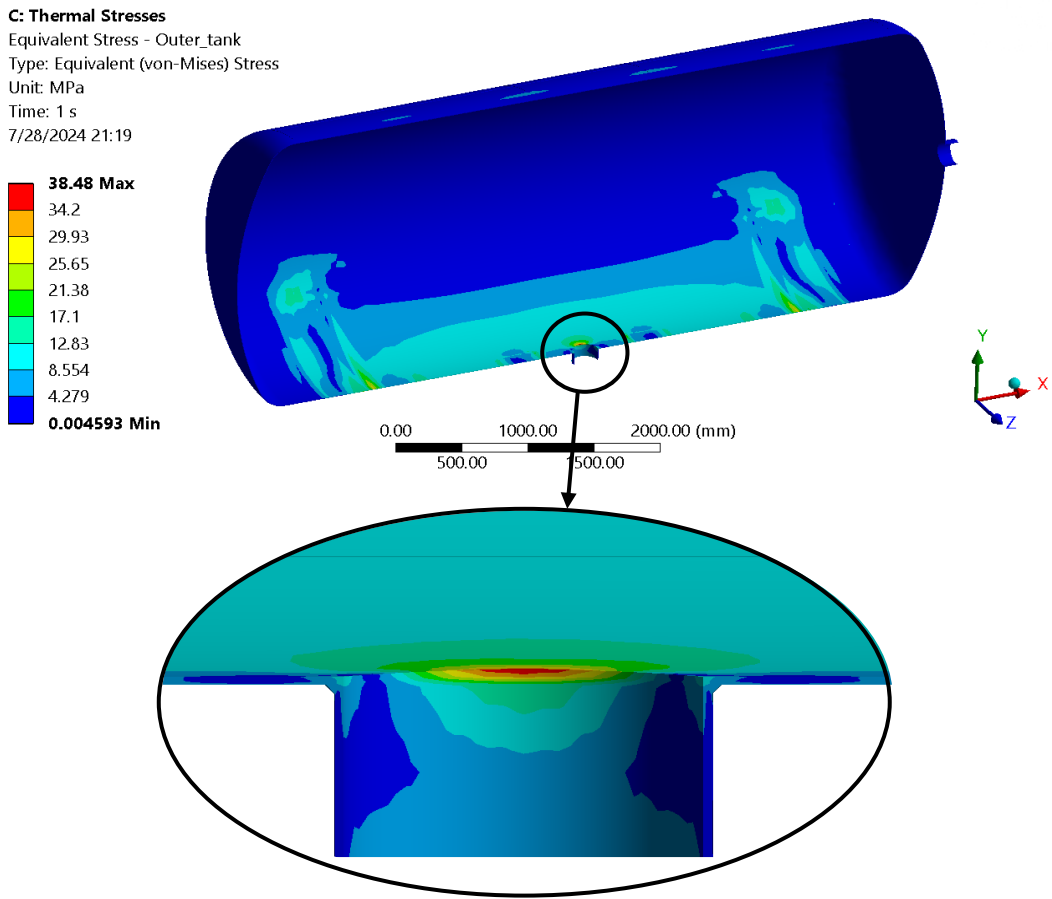
Figure 26. Stresses distribution in the outer tank due to thermal loads

Figure 27 displays the stress distribution of the inner tank. High stress values can be observed in the zone where the springs are connected to the tank, as occurred in the outer tank. The maximum stress value is 7.69 MPa and is located in the connection of the spring 8. In contrast to the outer tank, this tank has no components that restrict the thermal contraction or expansion

45

movements in this tank. Additionally, the stresses in the pipe's connection zone are lower and are evenly distributed between the tank and the reinforcement around the opening. As expected from the temperature distribution, stress values in the inner tank are lower than in the outer tank.
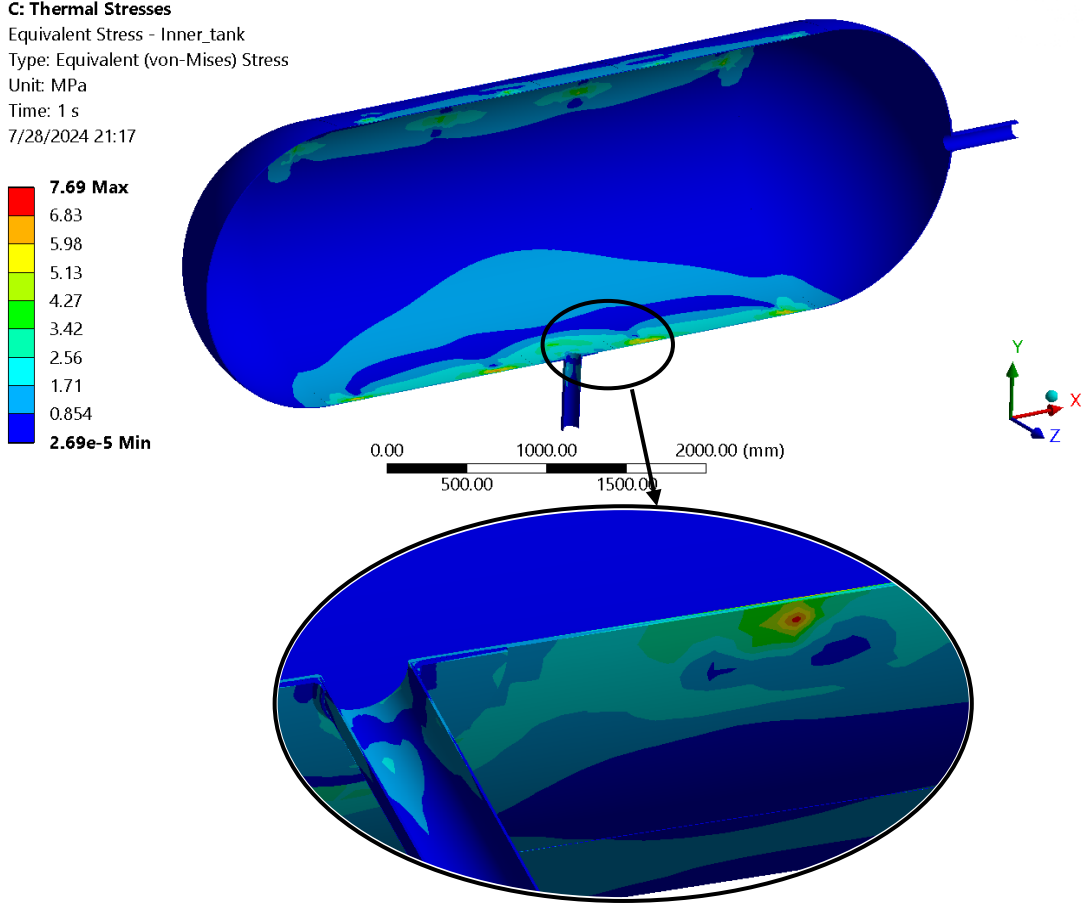
Figure 27. Stresses distribution in the inner tank due to thermal loads

The last component analyzed in this section is the spring arrangement of the LH2 storage unit. Using the thermal distribution to evaluate the stresses in the elements, the highest values are expected to happen to these elements. In Figure 28 shows the stress distribution for the spring number 11. This spring presented the maximum stress value among the 16 springs of the arrangement. This figure presents the spring in the isometric view to indicate the disposition of the spring in the tank. The maximum stress value is in the open ground end of the spring connected to the inner tank. This area has an important geometry change and movement due to thermal contraction or expansion is restricted by the connection with the tank. This condition is reported in all the springs of the system. Presenting an average maximum stress value of 373.32 MPa.

C: Thermal Stresses
VM Stress - Spring 11
Type: Equivalent (von-Mises) Stress
Unit: MPa
Time: 1 s
7/28/2024 21:30

384.61 Max
341.9
299.19
256.48
213.76
171.05
128.34
85.625
42.913
0.20055 Min
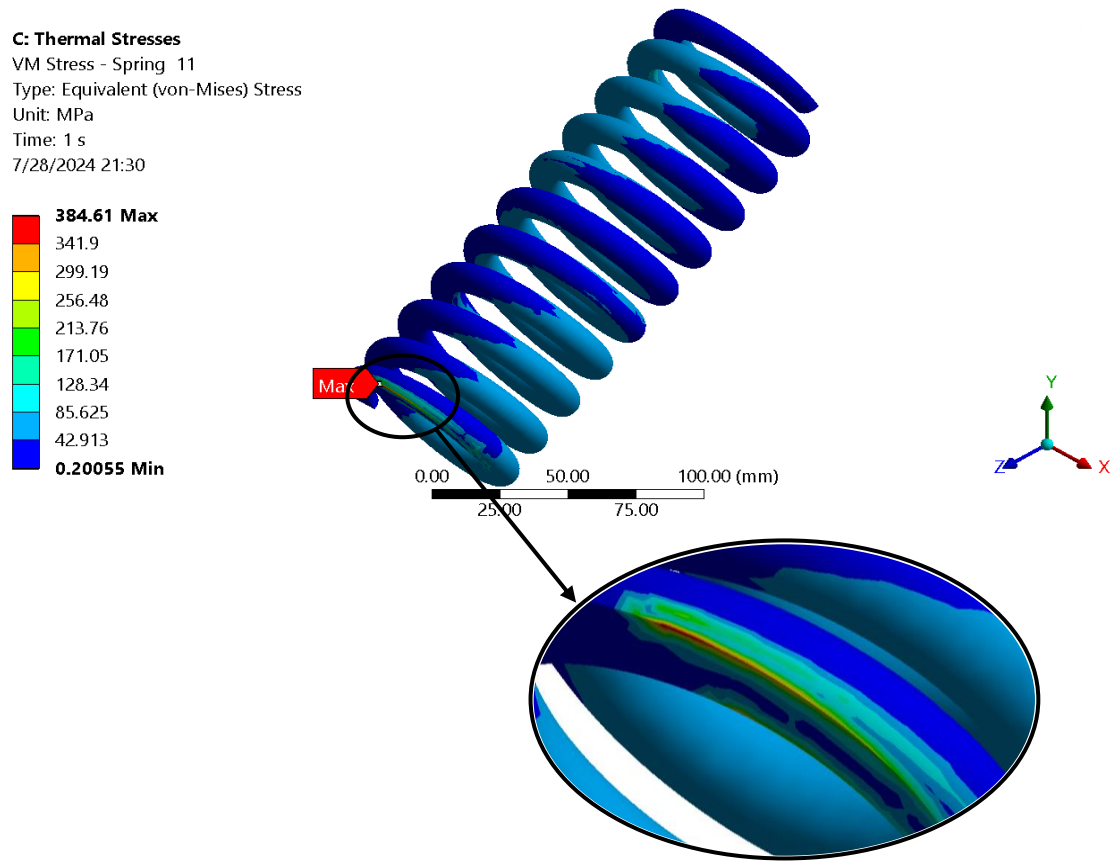
Figure 28. Stresses distribution in spring 11 due to thermal loads

The stress values generated because of the thermal loads on each component did not reach the yield stress of the material, which is 332 and 1300 MPa for the tanks and springs respectively. Once checked that there is no component failed, the evaluation of the bunkering loading case can be performed. The allowable stress values for the inner tank specified by the IGC code are addressed in the section 3.7.

3.6. Structural Analyses

This section is dedicated to the structural analyses carried out to compute the stress distribution generated by the two considered loading types. First, the bunkering loading condition related to the bunkering process is addressed. This process was done in one static structural numerical simulation considering the stress distribution results from the thermal analysis. The second study case is the ship's movement design loads. In the second case, three static structural simulations were performed, each one considering one of these accelerations: vertical, longitudinal, or transverse.

The stress distribution is presented for each of the components: outer tank, inner tank, and springs. For the spring arrangement, the results of two selected springs are presented: one representing the vertically aligned springs and another for the inclined group of springs. Both springs correspond to the maximum stress value among each characteristic group in the two loading scenarios. The results of the springs are presented in an isometric view to show the orientation of the springs within the assembly in Figure 31 and Figure 34.

3.6.1. Bunkering Loading Stress Distribution

This analysis was performed considering the general boundary conditions and the internal pressure in the inner tank surface as explained in the section 3.3.2. Additionally, the stresses obtained from the thermal analysis are considered for this analysis.

3.6.1.1 Outer Tank

The stress distribution in the outer tank is displayed in Figure 29. It can be noted from this figure that the stress values increase in the areas where the tank is connected to the springs or the legs. The maximum stress value, 71.81 MPa, occurs at the connection point of spring number 4. It can be observed that stress values are higher for the springs vertically aligned at the top of the tank, especially for springs 2 and 4 placed in the center of this row. High stress values in this area are explained by the combination of the shrinkage of the material due to the temperature drop (thermal stresses) and the weight of the inner tank and LH2 which tense the springs on the top.
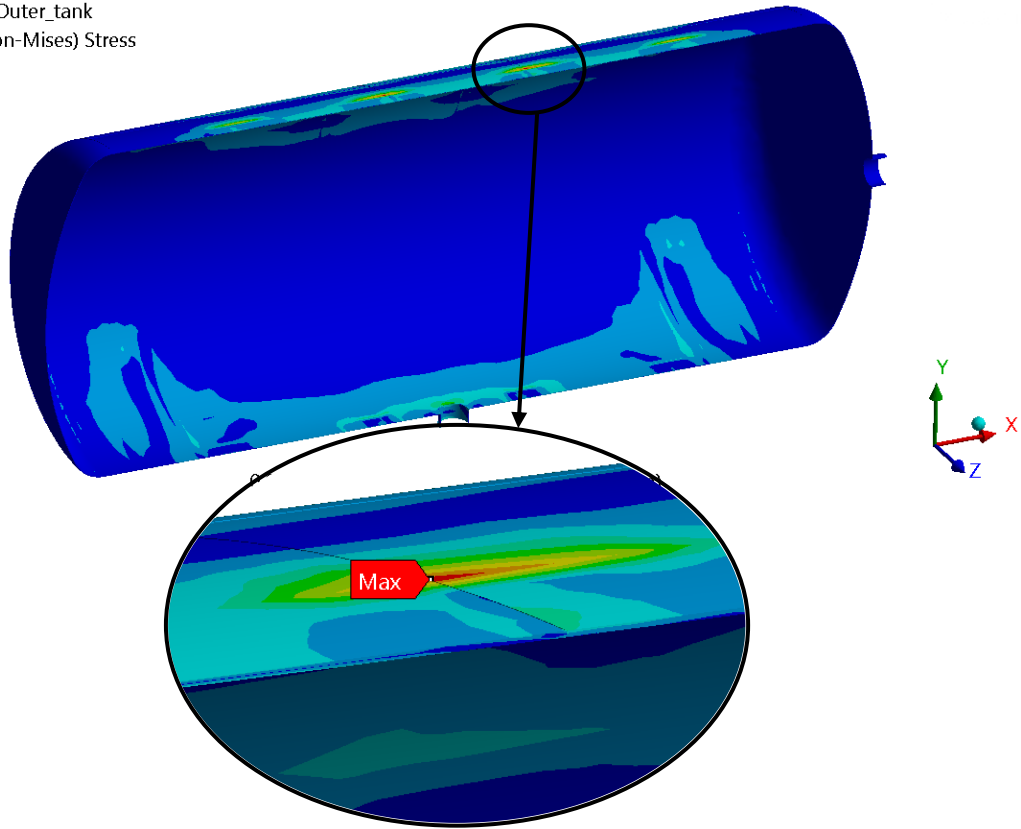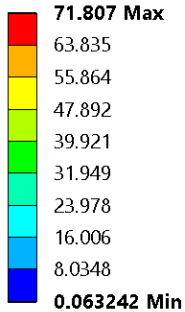
Figure 29. Stress distribution in the outer tank due to bunkering load case

3.6.1.2 *Inner Tank*

In the case of the inner tank, it shows an even stress distribution along its surface. Stresses are concentrated in the points where the springs are connected and at the edge of the opening for the tube at the bottom of the tank, where the maximum stress value of 126.82 MPa is located. The inner tank experienced an increment in temperature in the springs' connection points. Adding that dilatation effect to the internal pressure leads to an expansion of the material in the cylinder body of the tank. This expansion is limited by the stiffness of the springs, causing those longitudinal green spots in the tank, as shown in Figure 30.

49
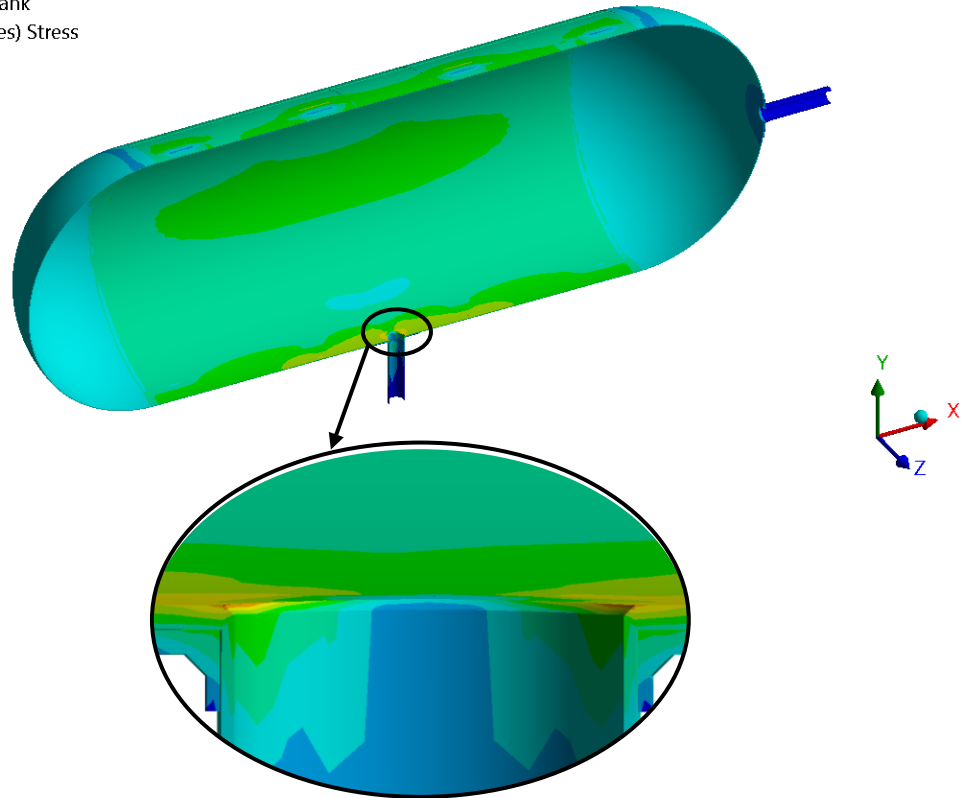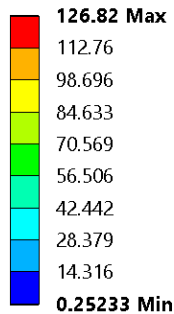
Figure 30. Stress distribution in the inner tank due to bunkering load case

3.6.1.3   Springs

Finally, the stress distribution of springs 3 and 10 is presented in Figure 31. Both springs are located at the top part of the arrangement. The stress distribution on these components is uneven and presents the maximum stress values concentrated in small spots near the end connected to the outer tank. maximum stress values are 944.83 and 952.62 MPa for springs 3 and 10 respectively. The average maximum stress value of the springs is 704.33 MPa. Considering their location, they are being stretched by the weight of the inner tank and LH2, leading to a tension state. However, according to their deformed shape, they are experiencing loads that are not axially aligned. Their complex loading condition might explain the uneven stress distribution and the stress concentrations at the ends of the springs.

(a) Spring 3   (b) Spring 10
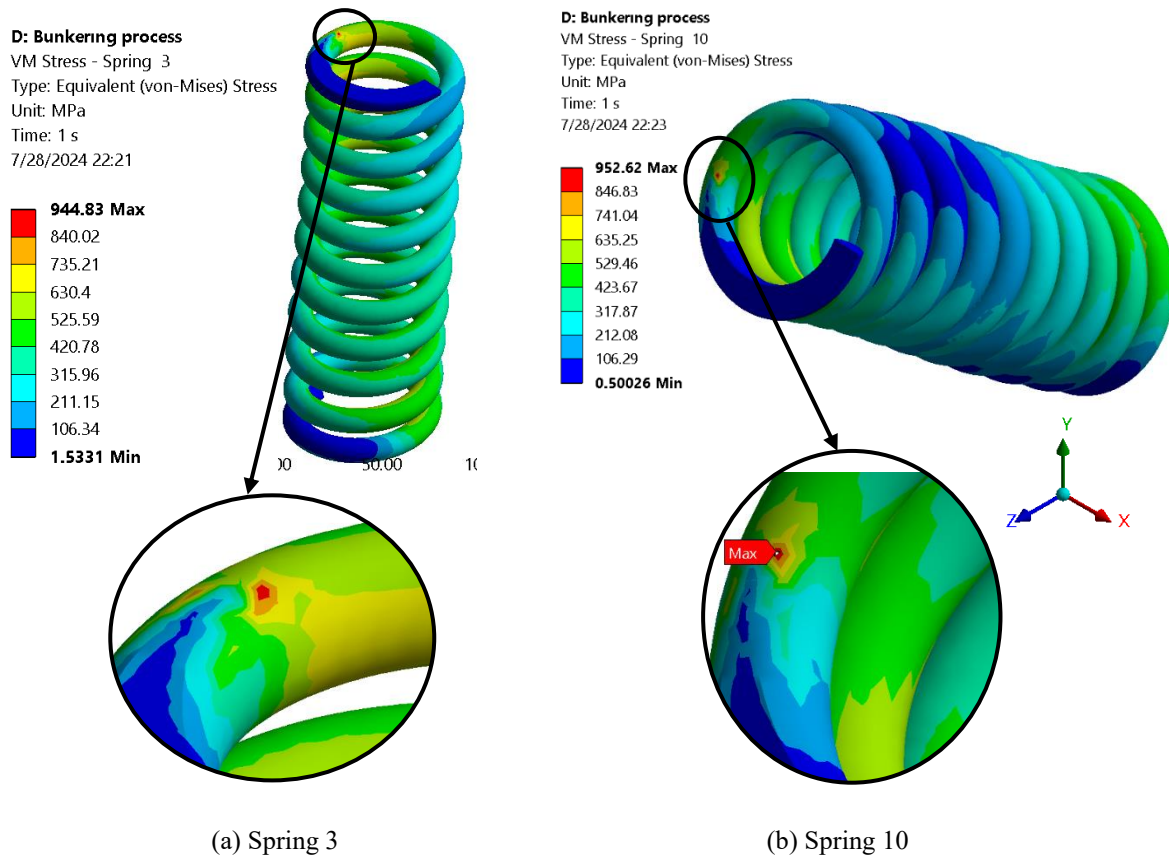
Figure 31. Stress distribution in springs 3 and 10 due to bunkering loading case

From the analysis of the components presented above, all the elements did not reach the yield stress of the corresponding material (see Table 2). Compliance with IGC code regulations for stress values and fatigue life assessment are discussed in sections 3.7 and 3.8.

3.6.2. Ship's Movement Loading Stress Distribution

The analysis of the ship's movement loading case is divided into three simulations associated with movements along vertical, longitudinal, and transverse directions. These study cases have similar conditions divided into general and case-related boundary conditions. The general boundary conditions explained in the section 3.3.2 are applied in all the simulations discussed in this section. In addition to the general boundary conditions, specific acceleration values were employed for each numerical analysis corresponding to the case-related boundary conditions. The study cases are longitudinal, vertical, and transverse accelerations which are characterized by the acceleration values in Table 5. The scenario presented corresponds to the vertical acceleration, as it generated the highest stress values among the three proposed study cases.

51

3.6.2.1 Outer Tank

Stresses produced in the outer tank of the LH2 storage unit by the vertical acceleration scenario are displayed in Figure 32. The stress distribution in the outer tank, including the location of the maximum stress, is similar to that observed in the bunkering loading case. Here, the maximum stress value is 100.9 MPa and matches the connection point of the spring 4. Stress increments are observed in the areas where the legs are connected, and around the piping hole located in the bottom of the cylinder body.
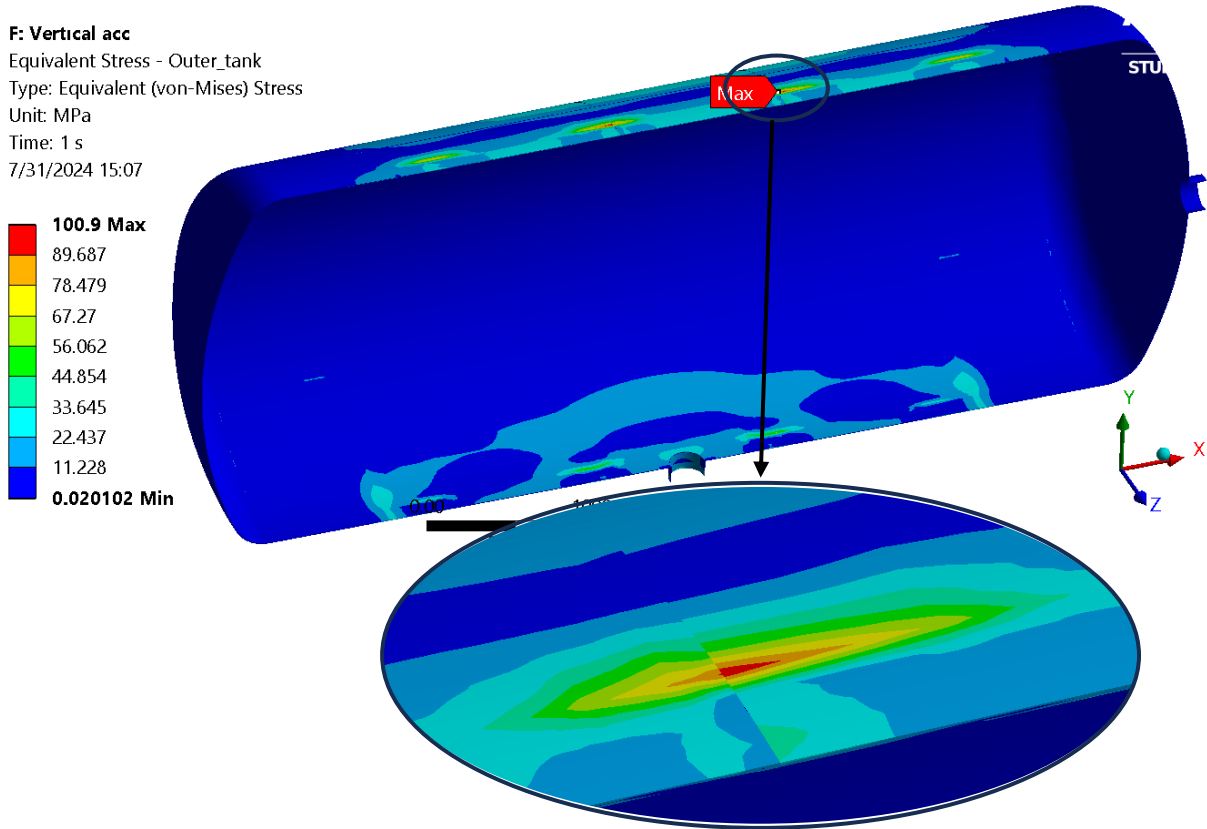
Figure 32. Stress distribution in the outer tank due to vertical acceleration

3.6.2.2 Inner Tank

For the inner tank, the stress distribution is shown in Figure 33. The inner tank for this loading condition reached a maximum stress value of 56.16 MPa, located at the connection with spring 7. It can be noted that stress values are higher around the springs located at the bottom of the tank than at the top. The load causing this behavior is the weight of the tank and LH2 since internal pressure was not considered in this scenario.
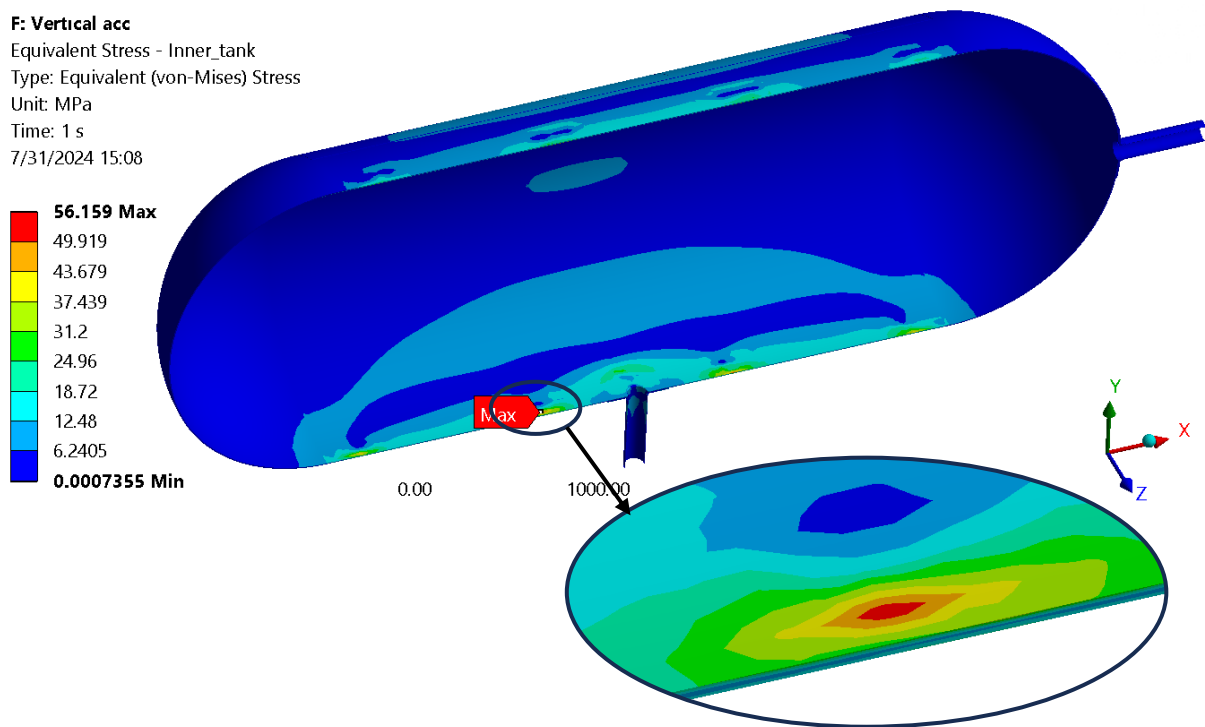
Figure 33. Stress distribution in the inner tank due to vertical acceleration

3.6.2.3 Springs

The springs with the highest stresses corresponding to the vertical and inclined configuration are presented in Figure 34. For the spring's group vertically aligned, spring number 8 shows a maximum stress value of 984.93 MPa close to the end connected to the inner tank. It has an even stress distribution with stress concentration spots on both ends. The spring is located at the bottom of the inner tank and experiences axial compressing loads characterizing this row with the same condition. This indicates that springs 1 to 4 vertically aligned at the top of the tank are subjected to tensile loading type.

The second spring presented is the number 9 and represents the springs with 60° of inclination from the vertical axis. This spring experiences a maximum stress value of 1183.7 MPa at the end connected to the inner tank. The stress distribution of this spring is uneven indicating that loads not axially aligned are affecting it, and thus all the inclined springs.

For this set of three numerical simulations, the maximum stress values experienced by the LH2 storage tank are below the yield strength of the materials, indicating that they will not fail due to the application of considered loads.
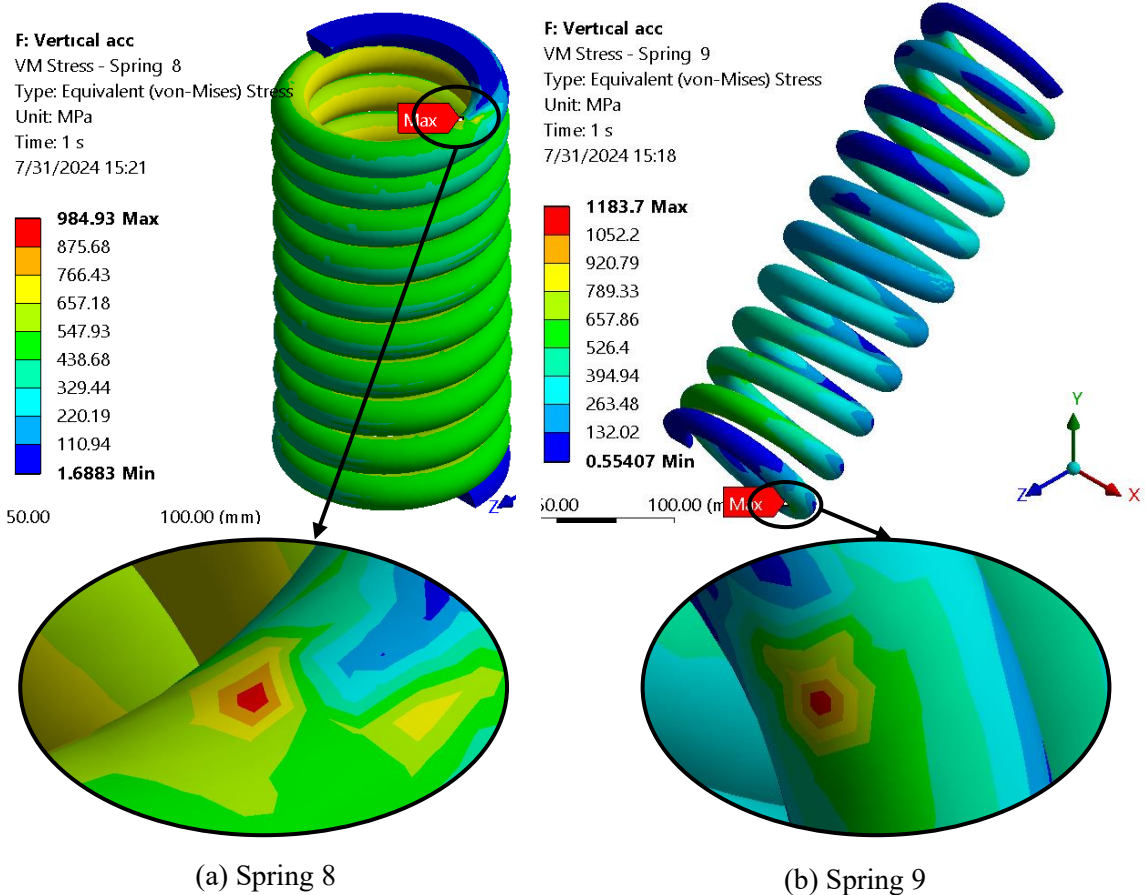
(a) Spring 8

(b) Spring 9

Figure 34. Stress distribution in springs 8 and 9 due to vertical acceleration

3.7. Tank's Stresses Regulation Compliance

The stress evaluation of the model and comparison with the material strength is used to identify whether or not each critical component of the LH2 storage unit will withstand or fail under the load conditions. However, this process alone is not sufficient to qualify the tank model under international regulations. The regulation referenced in this study, the IGC code, specifies stress limits for storage tanks. Specifically, limits related to shell elements bearing internal pressure.

The evaluation process requires the comparison of the stresses experienced by the tank storing a liquified gas with the stress values defined in the section 2.3.2 such as local and general membrane stresses, bending stress, and secondary stress. The regulation considers parameters related to the material to later set the maximum values based on the parameter f. Material properties and limits are presented in Table 7. Those regulations apply to the inner tank of the model presented in this research.

Table 7. Material information

Parameter	Value	Unit
Material	SS 316L	-
Yield Strength	332	[MPa]
Ultimate Strength	673	[MPa]
A	3.5	-
B	1.5	-
f	192.29	[MPa]
$1.5f$	288.43	[MPa]
$3f$	576.86	[MPa]

The stress types indicated in the evaluation process were obtained for each loading case in the FEA software. A path through the thickness of the inner tank wall was created and a linearized stress solution was set as output. The requested stress types are retrieved from the output file of this linear solution. Subsequently, different criteria for each stress type and the necessary combinations were calculated and contrasted with the standard. Table 8 summarizes the values and the status of each loading case. In summary, the inner tank passed all the acceptance criteria for pressurized tanks storing any liquified gases, LH2 for this study, established by the IGC code.

Table 8. Acceptance criteria for each load case

Criteria [MPa]	Loading type			
	Bunkering	Vertical accel.	Longitudinal accel.	Transverse accel.
$\sigma_m \leq f$	53.43	0.68	0.46	0.49
$\sigma_L \leq 1.5f$	83.00	12.57	9.59	11.53
$\sigma_b \leq 1.5f$	2.19	3.43	2.44	1.42
$\sigma_m + \sigma_b \leq 1.5f$	55.46	3.82	2.72	1.55
$\sigma_L + \sigma_b \leq 1.5f$	85.19	16.00	12.03	12.94
$\sigma_m + \sigma_b + \sigma_g \leq 3f$	100.53	7.98	5.78	4.66
$\sigma_L + \sigma_b + \sigma_g \leq 3f$	130.26	20.16	15.08	16.06
Status	Pass	Pass	Pass	Pass

3.8. Fatigue Analysis

After the stress evaluation using the allowable stress values set in the IGC code, the fatigue damage is analyzed for the three critical components in the bunkering and ship's movement loading conditions. The ship's movement loading condition is subdivided into the three acceleration cases presented in the structural analysis. To standardize the calculation process of the fatigue damage, curves corresponding to FAT71 and FAT160 were used for the tanks and springs respectively (see Figure 35). These FAT classes correspond to root crack applications in steel. FAT71 class is usually selected for steels with moderate fatigue strength limit, similar to the one selected for the inner tank (see Table 2), and has been used for fatigue damage analysis of type C tanks storing LNG (Park et al. 2021). FAT160 class corresponds to materials with high fatigue strength limit (Hobbacher 2016), as the one shown for the spring's steel in Table 2**Error! Reference source not found.**.

The results data presented for the springs corresponds to the average value of the 16 springs. Table 9 summarizes the values of fatigue damage, stress amplitude, design number of cycles, and number of cycles before failure. Stress amplitudes of the ship's movement loading scenario correspond to the average value of the different amplitudes proposed in section 2.3.4.
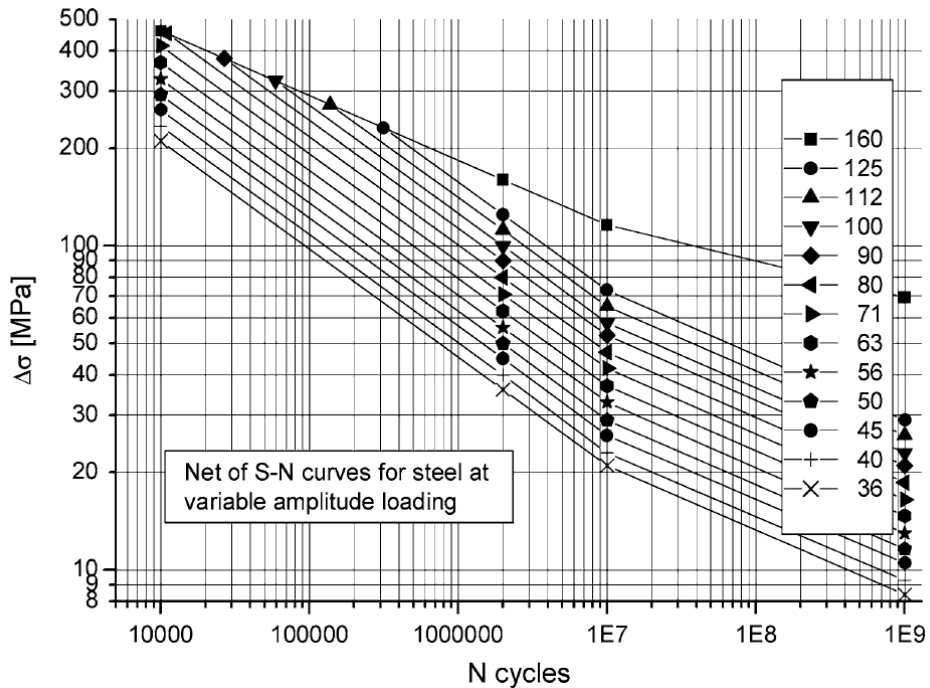
Figure 35. Modified resistance S-N curves of steel for Palmgren-Miner summation (Hobbacher 2016)

Fatigue damage computed in the outer tank shows that the bunkering loading case delivered more damage to this component than the ship's movement loading scenario. This can be explained by the larger stress amplitude experienced in this scenario. This trend is maintained for the inner tank, which experiences greater fatigue damage from the bunkering process compared to the ship's movement case. The internal pressure played an important role in this tank inducing a larger stress amplitude for this loading case compared to the outer tank. Both tanks comply with the limit of 0.1 fatigue damage specified by the IGC code.

The fatigue damage experienced by the springs is, on average, and for most of them, greater than 0.1. That condition exceeds the fatigue damage limit set by the IGC code. These elements will endure the expected number of cycles but do not comply with the regulation. It is noteworthy that the FAT160 class has a lower fatigue limit compared to the selected material of the springs. An additional comment on the fatigue damage of the springs is that high-stress values present in the springs are related to stress singularities located in their ends. This concern leaves room for further analysis and improvement in the spring arrangement design.

Table 9. Fatigue damage and stress amplitudes

Component	Load Case		σ_a [MPa]	n_i	N_i	Fatigue damage
Outer tank	Accel. design load	Longitudinal	4.66	9E+07	7.68E+27	1.17E-20
		Vertical	6.31	9E+07	1.00E+25	8.96E-18
		Transversal	4.95	9E+07	2.03E+27	4.44E-20
	Bunkering		32.17	1E+03	2.70E+09	3.70E-07
Inner tank	Accel. design load	Longitudinal	2.63	9E+07	2.33E+33	3.86E-26
		Vertical	3.51	9E+07	3.99E+30	2.26E-23
		Transversal	3.15	9E+07	4.39E+31	2.05E-24
	Bunkering		120.12	1E+03	4.13E+05	2.42E-03
Springs (av.)	Accel. design load	Longitudinal	53.17	9E+07	7.66E+08	2.39E-01
		Vertical	63.71	9E+07	2.26E+08	4.91E-01
		Transversal	49.16	9E+07	7.77E+08	1.30E-01
	Bunkering		331.01	1E+03	8.74E+05	7.51E-02

4. DISCUSSION

In this research, an extensive analysis was conducted on an LH2 type C tank, featuring a spring connection system between the main storage tank and the secondary barrier. The analysis evaluated the stresses experienced by the storage unit under two loading cases. The first one is the bunkering loading condition. Thermal numerical analysis was performed to evaluate the effects of the temperature gradient. Then, structural analyses were conducted to find the stress distribution. The second loading condition consisted of the evaluation of the stress distribution produced by the ship's design accelerations. From the results of the simulations, the following conclusions are drawn.

- The temperature distribution of the tank was computed considering the initial uniform temperature of the LH2 in the inner tank and the surroundings. Temperature variations in the inner and outer tank are less than 1°C and are concentrated in the places where the springs are connected. Because of the low-temperature gradient present in the tanks, their thermal stresses are also low. By contrast, the springs present a large temperature variation generating high stress values in these elements.

- The thermal simulation showed that the radiation heat transfer mechanism has an insignificant influence on the temperature of the inner tank. Moreover, just heat transfer through conduction in the springs was observed. As the contact surface of the springs is small. The spring connection design proved to reduce stresses in both tanks caused by temperature differences.

- The stress distribution for the type C tank was computed considering two loading conditions, bunkering and ship's movement loading study cases. The analysis of the results of these numerical simulations allowed the identification of the critical components with stress concentration areas. Furthermore, focused on the analysis and mesh refinement in those components saving computational resources in the process.

- In all the structural numerical simulations, the maximum stress value of the system is located in the springs. It is evident from the design (loads not aligned with the axis, number, and orientation of the springs); that the springs will present high stresses. However, additional reasons for this issue need to be considered. Stress singularities due to incorrect nodal coupling, and a finer mesh in the spring's ends need to be analyzed to improve the model.

- The load that induces high-stress values in the bunkering loading case is the vapor pressure for the inner tank. For the outer tank, the structure's weight is the dominant load. For the ship's movement loading case, the vertical acceleration resulted in the largest stress values.

- The storage unit complies with the allowable stress limits for its type. Regarding the fatigue damage, both tanks also comply with the rule limits. However, the springs do not satisfy the fatigue damage limit but withstand the expected number of cycles.

5. RECOMMENDATIONS AND FUTURE WORK

This section is dedicated to the recommendations based on the findings of the work. On top of that, suggestions for future work projects are presented. Within the analysis of the mechanical strength and fatigue endurance of the LH2 type C tank characterized by the novel spring connection arrangement, several key insights are proposed based on the problems faced along the methodology. These points will help to enhance the design and lead to new projects.

- Within the geometry preprocessing, divisions were performed in the tank to facilitate the meshing control and refine the mesh in areas of interest. This approach could be applied to the springs. Divide each spring into segments and define a finer mesh in the ends. For segments of the spring's body, a coarser mesh can be used to reduce the number of finite elements.

- A related recommendation to the previous one is to prioritize using the shared topology option over the bonded contact connection whenever possible. Computational resources will be saved by applying this point.

- The implementation of an automatic meshing and convergence check tool will help to achieve an optimal mesh in a short period.

Following with the future works based on this research, the next aspects can be addressed to continue with this project and improve the results:

- Modification in the spring arrangement to withstand the combined loading type. Changes in the position, design, or number of springs. If more springs are added, the design is modified to increase the diameter of the wire or contact area, it is expected to increase the heat transfer to the inner tank. implementations of insulation materials instead in the space between tanks can be studied to palliate the heat transfer increment.

- Performing CFD analysis to retrieve the real temperature distribution, the evaporation model, and the boil-off effect resulting in more accurate values of pressure and stress distribution. Additionally, with the CFD analysis, the free surface effect of the LH2 inside the tank can be included and evaluate its influence on the stress distribution.

- Finally, the LH2 type C tank can be evaluated under different collision scenarios.

6. ACKNOWLEDGEMENTS

First and foremost, I would like to express my deepest gratitude to my parents for the unconditional support you have given me throughout every day of this stage of my life. Knowing that I can always count on your help for every challenge I face has been invaluable. This achievement is as much yours as it is mine, for you never let me give up from the distance. Your dedication and effort have enabled me to keep moving forward and strive to be better, not just as a professional, but more importantly, as a person. I hope that this accomplishment can, in some small way, repay the immense effort and support you have given me.

"Porque todos los logros alcanzados no vienen de una sola persona, porque los esfuerzos realizados no pudieron ser posibles sin su aliento cada paso dado representa las ilusiones y deseos de superación. A mi familia por todo su apoyo y por el que vendrá…"

I am also grateful to the DLR team for providing me with the opportunity to pursue this research. Thanks to my colleagues and supervisors for the feedback and guidance during this process.

I would like to extend my appreciation to Rostock University, Liège University, EMship+, and Professor Philippe Rigo for providing me the opportunity to be part of this program and for all the invaluable experiences.

Finally, I would like to acknowledge all my friends and peers who have been part of this journey. Your companionship has made this experience truly memorable.

7. BIBLIOGRAPHY

Abinay; Venkatesh, C.; Vishnuvardhan, Sanka (2022): Design and Analysis of Hydrogen Storage Tank with Different Materials by Using Ansys. In: *International Journal of Research Publication and Reviews* 3 (7), S. 835–838. Online available on https://ijrpr.com/uploads/V3ISSUE7/IJRPR5732.pdf.

Aijjou, A. (2019): Influence of Solar Energy on Ship Energy Efficiency: Feeder Container Vessel as Example. In: *International Journal of Electrical Energy* 7 (1), S. 21–25.

IGC Code, 22.05.2014: AMENDMENTS TO THE INTERNATIONAL CODE FOR THE CONSTRUCTION AND EQUIPMENT OF SHIPS CARRYING LIQUEFIED GASES IN BULK (IGC CODE).

Ansys, Inc (2023): Ansys Workbench. Version 2023 R1: Ansys, Inc.

Balat-Pichelin, M.; Sans, J. L.; Bêche, E. (2022): Spectral directional and total hemispherical emissivity of virgin and oxidized 316L stainless steel from 1000 to 1650 K. In: *Infrared Physics & Technology* 123, S. 104156. DOI: 10.1016/j.infrared.2022.104156.

Besten, Henk den (2018): Fatigue damage criteria classification, modelling developments and trends for welded joints in marine structures. In: *Ships and Offshore Structures* 13 (8), S. 787–808. DOI: 10.1080/17445302.2018.1463609.

Bo Wang (Hg.) (2015): Strength Assessment of Type `C' LNG Fuel Tanks. International Conference on Ocean, Offshore and Arctic Engineering. Newfoundland, Canada, May 31-June 5. ASME.

Cotorcea, Alexandru; Ozkaynak, Suleyman (2014): PRESENT AND FUTURE OF RENEWABLE ENERGY SOURCES ONBOARD SHIPS. CASE STUDY: SOLAR – THERMAL SYSTEMS. In: *"Mircea cel Batran" Naval Academy Scientific Bulletin* 17 (1), S. 35–39.

DNV-RU-SHIP: DNV-RU-SHIP Pt.4 Ch.7 Pressure equipment.

Du-Yong Lee; Jae-Sang Jo; Antony John Nyongesa and Won-Ju Lee (2023): Fatigue Analysis of a 40 ft LNG ISO Tank Container. In: *Materials* 16 (1).

EngineerExcel: Compression Spring Formulas: A Complete Guide. Hg. v. EngineerExcel. Online available on https://engineerexcel.com/compression-spring-formula/.

Foretich, Anthony; Zaimes, George G.; Hawkins, Troy R.; Newes, Emily (2021): Challenges and opportunities for alternative fuels in the maritime sector. In: *Maritime Transport Research* 2, S. 100033. DOI: 10.1016/j.martra.2021.100033.

Fricke, Wolfgang (2017): Fatigue and Fracture of Ship Structures. In: John Carlton, Paul Jukes und Yoo Sang Choo (Hg.): Encyclopedia of Maritime and Offshore Engineering: Wiley, S. 1–12.

Hobbacher, A. F. (2016): Recommendations for Fatigue Design of Welded Joints and Components. 2nd ed. 2016. Cham: Springer International Publishing; Imprint: Springer (IIW Collection).

Kim, Myung-Sung; Chun, Kang Woo (2023): A Comprehensive Review on Material Compatibility and Safety Standards for Liquid Hydrogen Cargo and Fuel Containment Systems in Marine Applications. In: *Journal of Marine Science and Engineering* 11 (10), S. 1927. DOI: 10.3390/jmse11101927.

DNV-CG-0135, 12/2023: Liquefied gas carriers with independent cylindrical tanks of type C.

Liu, Yinhua; Zhou, Peilin; Jeong, Byongug; Wang, Haibin (2023): Design and optimization of a type-C tank for liquid hydrogen marine transport. In: *International Journal of Hydrogen Energy* 48 (89), S. 34885–34896. DOI: 10.1016/j.ijhydene.2023.05.102.

Marzbanrad, Javad; Paykani, Amin; Afkar, Amir; Ghajar, Mostafa (2012): Finite element analysis of composite high-pressure hydrogen storage vessels. School of Automotive Engineering. Tehran. Online available on https://www.jmaterenvironsci.com/Document/vol4/8-JMES-286bis-2012-Paykani.pdf.

Mohammad, K. A.; Ali, Aidy; Sahari, B. B.; Abdullah, S. (2012): Fatigue behavior of Austenitic Type 316L Stainless Steel. In: *IOP Conf. Ser.: Mater. Sci. Eng.* 36, S. 12012. DOI: 10.1088/1757-899X/36/1/012012.

Niemi, Erkki; Fricke, Wolfgang; Maddox, Stephen J. (2018): Structural Hot-Spot Stress Approach to Fatigue Analysis of Welded Components. Designer's Guide. 2. Aufl.: Springer Nature (IIW Collection).

Park, Junesung; Lee, Jungyup; Kim, Minsung; Eun, Hyeonjun; Hong, Sorang (2023): Research Report of Material Compatibility for Liquid Hydrogen Storage on Marine Application. Koren Register; Korean Institute of Machinery and Materials; Pusan National

University. Busan. Online available on
https://www.krs.co.kr:443/eng/Exclusive/Tech_ETC_View.aspx?MRID=546&NO=3535.

Park, Young-IL; Cho, Jin-Seong; Kim, Jeong-Hwan (2021): Structural Integrity Assessment of Independent Type-C Cylindrical Tanks Using Finite Element Analysis: Comparative Study Using Stainless Steel and Aluminum Alloy. In: *Metals* 11 (10), S. 1632. DOI: 10.3390/met11101632.

Ratnakar, Ram R.; Gupta, Nikunj; Zhang, Kun; van Doorne, Casimir; Fesmire, James; Dindoruk, Birol; Balakotaiah, Vemuri (2021): Hydrogen supply chain and challenges in large-scale LH2 storage and transportation. In: *International Journal of Hydrogen Energy* 46 (47), S. 24149–24168. DOI: 10.1016/j.ijhydene.2021.05.025.

San Marchi, C.; Dedrick, D. E.; van Blarigan, P.; Somerday, B. P.: PRESSURE CYCLING OF TYPE 1 PRESSURE VESSELS WITH GASEOUS HYDROGEN. Sandia National Laboratories. Livermore CA. Online available on https://h2tools.org/sites/default/files/2019-08/paper_148.pdf.

Senthil Kumar, S.; Bibin, C.; Ramachandran, M. (2020): Design and Analysis of Hydrogen Storage Tank with Different Materials by Ansys. In: *IOP Conf. Ser.: Mater. Sci. Eng.* 810 (1), S. 12016. DOI: 10.1088/1757-899X/810/1/012016.

Tomioka, Jun-ichi; Kiguchi, Kazuhiro; Tamura, Yohsuke; Mitsuishi, Hiroyuki (2012): Influence of pressure and temperature on the fatigue strength of Type-3 compressed-hydrogen tanks. In: *International Journal of Hydrogen Energy* 37 (22), S. 17639–17644. DOI: 10.1016/j.ijhydene.2012.05.045.

Ueno, H.; Kakihata, K.; Kaneko, Y.; Hashimoto, S.; Vinogradov, A. (2011): Enhanced fatigue properties of nanostructured austenitic SUS 316L stainless steel. In: *Acta Materialia* 59 (18), S. 7060–7069. DOI: 10.1016/j.actamat.2011.07.061.

UNCTAD (2018): REVIEW OF MARITIME TRANSPORT - 2018. Unter Mitarbeit von Jan Hoffmann und Juan Wendy. UNCTAD. Online available on https://archive.org/details/85294/mode/2up.

Wang, Yifan; Wright, Laurence A. (2021): A Comparative Review of Alternative Fuels for the Maritime Sector: Economic, Technology, and Policy Challenges for Clean Energy Implementation. In: *World* 2 (4), S. 456–481. DOI: 10.3390/world2040029.

Weicheng, Cui (2002): A state-of-the-art review on fatigue life prediction methods for A state-of-the-art review on fatigue life prediction methods for metal structures. In: *Journal of Marine Science and Technology*, S. 44–55.

Zhou, Chilou; Li, Zhiyuan; Zhao, Yongzhi; Hua, Zhengli; Ou, Kesheng; Zhang, Lin et al. (2016): Design fatigue life evaluation of high-pressure hydrogen storage vessels based on fracture mechanics. In: *Proceedings of the Institution of Mechanical Engineers, Part E: Journal of Process Mechanical Engineering* 230 (1), S. 26–35. DOI: 10.1177/0954408914537485.

APPENDICES

A1. Maximum von Mises stress at each spring due to the bunkering process

	Maximum von Mises stress [MPa]	
	Bunkering loading case	
Spring #	Thermal Stresses [MPa]	Thermal + Pressure [MPa]
1	365.38	598.77
2	364.54	561
3	379.91	944.83
4	380.63	826.49
5	381.59	501.85
6	381.78	578.76
7	365.27	514.95
8	366.04	617.93
9	380.85	949.81
10	380.07	952.62
11	384.61	859.74
12	378.4	850
13	362.8	649.64
14	368.85	587.26
15	366.07	671.45
16	366.29	604.14

A2. Maximum von Mises stress at each spring due to the ship's movement loading condition

Spring #	Maximum von Mises stress [MPa]		
	Ship's movement loading case		
	Longitudinal accel.	Vertical accel.	Transverse accel.
1	681.07	933.23	765.55
2	686.16	924.15	759.43
3	971.45	922.53	758.1
4	918.37	885.71	731.03
5	976.5	954.17	773.03
6	978.94	921.59	753.71
7	766.83	953.23	740.68
8	809.99	984.93	776.79
9	1079.4	1183.7	902.51
10	1005.8	1056	753.23
11	1029	1160.1	880.66
12	973.3	1051.2	748.21
13	706.5	1143.7	865.05
14	695.64	1048.9	757.53
15	674.33	1144.6	870.36
16	658.46	1041.3	749.69